

Counting currents: resolving contradictory records of eruption history created by unsteady pyroclastic density current dynamics

Natasha J. Dowey (née Smith)*¹, Richard J. Brown² and B. Peter Kokelaar³

¹ Geography, Environment and Planning, Sheffield Hallam University, Sheffield, UK

² Department of Earth Sciences, Durham University, Durham, UK

³ Department of Earth Sciences, Durham University, Durham, UK

* N.Dowey@shu.ac.uk [corresponding author]

*This is a non-peer reviewed preprint submitted to EarthArxiv.
Feel free to contact the lead author, we welcome your feedback.*

Counting currents: resolving contradictory records of eruption history created by unsteady pyroclastic density current dynamics


Natasha J. Dowey (née Smith)*¹, Richard J. Brown² and B. Peter Kokelaar³

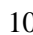
¹ Geography, Environment and Planning, Sheffield Hallam University, Sheffield, UK

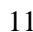
² Department of Earth Sciences, Durham University, Durham, UK

³ Department of Earth Sciences, Durham University, Durham, UK

* N.Dowey@shu.ac.uk [corresponding author]

 ORCID (NJD): 0000-0002-9231-4781

 ORCID (RJB): 0000-0002-7415-9490

 ORCID (BPK): 0000-0002-2452-703X

Keywords: Stratigraphy; Correlation; Volcanic Hazard; Unsteadiness; Uncertainty; Volcanology

Abstract

Ignimbrite lithofacies analysis can be used to interpret the number and behaviour of pyroclastic density currents (PDCs) generated during a Plinian eruption, through identification of flow units in the rock record. However, pyroclastic stratigraphic successions are rarely complete and without breaks around a volcano, complicating regional analysis of hiatus markers. This study uses entrachron correlation to reconcile conflicting proximal and distal lithofacies architecture of the 273 ka Poris Formation, Tenerife, to reveal a coherent eruption history. The novel correlation illustrates that hiatus in PDC activity can vary spatially and rapidly due to regional-scale unsteadiness and non-uniformity in PDC dynamics. Distal stratigraphy may not accurately record the number of PDCs generated during an eruption and breaks in ignimbrite deposition do not necessarily imply discontinuous PDC development. These findings bear importantly on hazard inferences derived from ignimbrite lithofacies successions, and have significance for numerical and experimental modelling of unsteadiness in granular flows.

1. Introduction

Pyroclastic density currents (PDCs) generated during explosive volcanic eruptions are flows of volcanic ash, gas and rock that can reach internal temperatures of $>500^{\circ}\text{C}$, travel at speeds of $>200\text{ ms}^{-1}$ and cover vast areas (e.g., Fisher, 1966; Sparks, 1976; Fisher & Schmincke, 1984; Wilson, 1985; Branney & Kokelaar, 1992, 2002; Druitt, 1998; Sulpizio et al., 2014; Dufek et al., 2015; Lube et al., 2020). In their wake they leave complex deposits on the ground, here referred to as ignimbrites. During Plinian eruptions, ignimbrite sheets may build up, composed of several ignimbrite units interbedded with pumice or ash fall deposits (e.g., Pittari et al., 2006; Dávila Harris et al.,

33 2013; Cavazos-Álvarez & Carrasco-Núñez, 2020). Interpretation of ignimbrite stratigraphy has been crucial in
34 developing understanding of how these deadly hazards behave in time and space, and in unpicking eruption
35 histories of the events that generate them (e.g., Cas & Wright, 1987; Fisher et al., 1993; Branney & Kokelaar, 1997;
36 Lube et al., 2007; Silva Parejas et al., 2010; Williams et al., 2014).

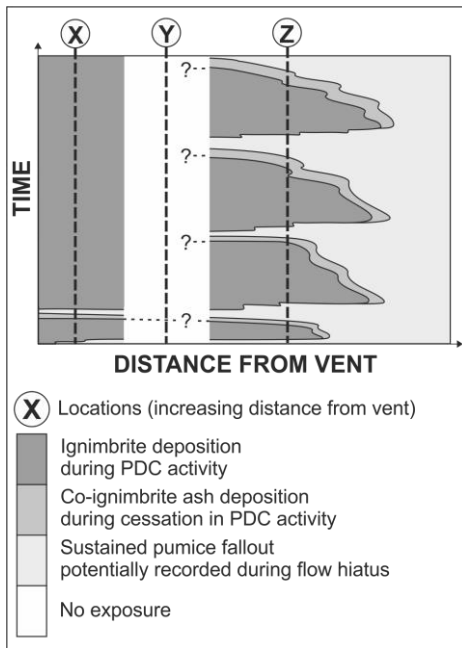
37

38 Although a critical tool, ignimbrite analysis is not straightforward. Pyroclastic stratigraphy is rarely complete;
39 proximal exposures may be missing or obscured due to destruction during caldera collapse (e.g., Gooday et al.,
40 2018), bypass may lead to non-deposition (e.g., Brown & Branney, 2004), changes in eruption conditions may lead
41 to syn-eruption scour and erosion (e.g., Gase et al., 2017), syn-eruption reworking may influence stratigraphic
42 architecture (e.g., Wilson & Hildreth, 1998; Myers et al., 2016), and post-eruption erosion may lead to disconnected
43 outcrops (Mues-Schumacher & Schumacher, 1996). Furthermore, Plinian eruptions are complex; different
44 processes may be operating at different distances from the vent (e.g., Houghton et al., 2004), and pyroclastic density
45 currents are inherently unsteady and non-uniform in time and space (Branney & Kokelaar, 2002). Stratigraphic
46 clues may seem contradictory at different locations around the volcano unless a full enough record is present to
47 bring together a coherent story (Fig. 1). Such factors can lead to uncertainty in our interpretations of how many
48 PDCs were formed during an eruption, how far each travelled, their internal dynamics, and how they interacted
49 with the environment, impacting our ability to confidently interpret eruption histories and understand future
50 potential hazard.

51

52 This study explores how our interpretation of the number of PDCs generated during an eruption, as recorded by
53 stratigraphic ‘flow units’, can be shaped by outcrop location and internal PDC dynamics. We correlate well-
54 documented proximal (N. Smith & Kokelaar, 2013) and distal (Brown & Branney, 2004b, 2013) stratigraphic
55 counterparts of the 273 ka Poris ignimbrite of Tenerife to interrogate factors influencing contradictory equivalent
56 stratigraphy. We then discuss the implications of this work for uncertainty in field interpretations of ignimbrite
57 successions and volcanic hazard analysis.

58



59

60 **Figure 1: Schematic showing how flow units could be interpreted differently at different locations from the vent,**
 61 **dependent on the nature of preserved ignimbrite stratigraphy. At location X, two flow units are recorded. At location**
 62 **Z, four flow units are recorded. At location Y, there is no exposure, complicating correlation of flow units. Adapted**
 63 **after Branney and Kokelaar (2002).**

64 1.1 Flow units and episodes of PDC hiatus

65 A ‘flow unit’ in ignimbrite stratigraphy is most simply defined as a stratigraphic package that records the passage
 66 of a single pyroclastic density current (Sparks, 1976). The term has been used for many years (e.g., Ross & Smith,
 67 1961), although how we identify and define flow units has evolved through time.

68

69 In 1973, Sparks et al. proposed a “standard ignimbrite flow unit” paradigm, where changes in bedding, grading and
 70 pumice concentration were used to distinguish the deposits of discrete pyroclastic currents that came to a halt en
 71 masse (Sparks et al., 1973; Sparks, 1976). It is now understood that PDCs aggrade progressively from the flow
 72 boundary zone, which includes the lowermost part of the current and the uppermost part of the forming deposit
 73 (Fisher, 1966; Branney & Kokelaar, 2002). In this progressive aggradation model, a flow unit can comprise a wide
 74 spectrum of stratigraphic bedforms. Bedding and grading changes within an ignimbrite reflect the unsteadiness of
 75 PDC conditions through time, recording changes in conditions at the flow boundary zone (Branney & Kokelaar,
 76 2002). Flow units may be recognised by well-defined upper and lower boundaries or may contain distinctive

77 assemblages of clasts (as in Silva Parejas et al., 2010), but evidence of clear hiatus in current activity, rather than a
78 particular stratigraphic sequence, is key in delineating flow units and discrete density current events.
79
80 Plinian fallout layers, evidence of secondary reworking or soil within an ignimbrite sequence may all provide robust
81 evidence for a hiatus in PDC activity (e.g. Cavazos-Álvarez & Carrasco-Núñez, 2020). Ash layers correlated across
82 large distances within ignimbrite successions can also record episodes of hiatus, where deposition of co-ignimbrite
83 ash occurs after passage of a pyroclastic density current (e.g., Sparks & Walker, 1977; Sigurdsson & Carey, 1989;
84 Brown & Branney, 2004b; Pittari et al., 2006). It is important to distinguish between no current activity at all, and
85 temporarily redirected current activity that would form a local hiatus. A hiatus in one place could reflect momentary
86 lateral redirection of a current owing to rapid changes at the vent, changes in PDC dynamics and run out distance,
87 or topographic effects; factors we will discuss below.

88 **1.2 Correlating ignimbrite lithofacies**

89 To fully understand the evolution of PDC behaviour in time and space, and to correlate episodes of hiatus and
90 therefore flow units within a single eruption, a time-geometry framework is required (Branney & Kokelaar, 2002).
91 The deposition of lithofacies and compositional zones across an ignimbrite extent may be diachronous (e.g.,
92 Wilson & Hildreth, 1997) and physical similarities between ignimbrite lithofacies are unlikely to represent temporal
93 correlation; lithostratigraphy does not necessarily equate to chronostratigraphy. In compositionally zoned
94 ignimbrite sheets that record systematic changes in magma chemistry through time, geochemical correlation is an
95 important correlative tool in revealing spatial and temporal variations in PDC behaviour (e.g., Fierstein & Wilson,
96 2005; Williams et al., 2014). But in ignimbrites that lack high-resolution geochemical variation, other methods are
97 needed. Branney and Kokelaar (2002) introduced the term ‘depochron’ for a notional surface within an ignimbrite
98 sheet connecting clasts deposited from the current at the same moment in time. However over large distances, with
99 a lack of connecting exposure and significant changes in outcrop appearance, depochrons can be difficult to
100 establish. ‘Entrachrons’ are notional surfaces connecting the lowermost clasts that were *entrained into the current*
101 together at the same instant in time; they may be marked, for example, by the first appearance of a new type of
102 pumice or lithic clast within the stratigraphy (Branney and Kokelaar, 2002). Such entrachrons need not occur in
103 the same lithofacies in different areas (this would depend on the conditions of the flow boundary zone of the PDC
104 at each location). In this study, we use entrachron analysis to aid correlation of distinct ignimbrite lithofacies and
105 flow units.

106

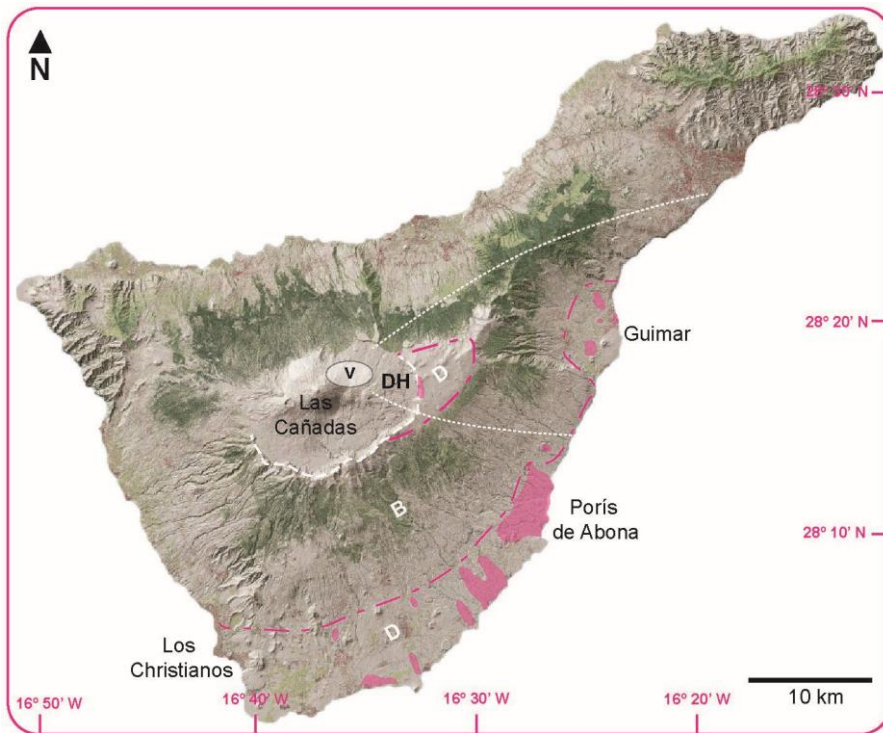
2. Case study: the 273 ka Poris ignimbrite, Tenerife

2.1 Geological setting

Tenerife is a large shield volcano, with diverse volcanic products recording the interspersed remnants of basaltic shield volcanism from three volcanic rift zones (~12 Ma – 3 Ma), central pyroclastic activity (~3 Ma – 0.7 Ma), and monogenetic flank volcanoes and tuff rings (Ancochea et al., 1990, 1999; Martí et al., 1994; Bryan et al., 1998, 2000; Brown et al., 2003; Edgar et al., 2007; Cas et al., 2022; Dávila Harris et al., 2023).

The centre of the island is dominated by Las Cañadas depression (Fig. 2), which contains the present-day Teide-Pico Viejo stratovolcano and is partly encircled by a ~27 km-long wall comprising strata representing 3 Ma of volcanic activity (Martí et al., 1994; Martí, 2019). These strata become successively younger from the western Ucanca sector, through the central Guajara sector, to the eastern Diego Hernandez (DH) wall. The DH wall is the “proximal” area of this study. It is ~1.9 km long and 180–240 m high, orientated N–SSW, and exposes proximal ignimbrite deposits intercalated with lava flows, scoria cones and sedimentary strata. These deposits occur within a palaeovalley (Martí et al., 1990) bounded by the Risco Verde escarpment to the south and monogenetic scoria cones and lavas of the Cordillera Dorsal to the north. Bedding within the upper pyroclastics dips consistently at ~2° ESE, indicating that the lava substrate had a low topographic profile. Within approximately 3 km of the wall, the topography of the volcano consists of steep flanks up to 10–20°. This medial zone contains hardly any ignimbrite exposure.

In this study, the “distal” Bandas del Sur region refers to an 180° sector of the southern flanks of the volcano, stretching from the Güimar valley to Los Cristianos (Fig. 2). This region is broadly concave, extending from the steep medial flanks to lower gradient (6°) coastal flanks that reach ~5 km inland and range from 15–20 km wide. Extensive ignimbrite deposits across this part of the island record at least twelve inferred caldera-forming events, indicating that multiple stratovolcanoes have been constructed and destroyed during the island’s history (Bryan et al., 1998, 2000; Brown et al., 2003; Edgar et al., 2007; Dávila Harris et al., 2023). The Bandas del Sur has a semi-arid climate prone to flash floods, and the slopes of the volcano are incised with a network of deep radial valleys. Palaeotopography indicates that the region has had a similar topography for the past 2 Ma (Pittari et al., 2006).



135

136

137

138

Figure 2: Map of outcrops of Poris ignimbrite (pink). Pink dashed line separates zones of deposition (D) and bypassing (B) (Brown and Branney, 2013). V = vent from Edgar et al., (2004). White dotted line is 50 cm Poris isopach from Edgar et al., (2004). DH = Diego Hernandez.

139

2.2 The contrasting records of the 273 ka Poris Ignimbrite

140

141

142

143

144

145

The 273 ka Poris event is one of the largest Quaternary Plinian eruptions recorded on Tenerife (Brown et al., 2003; Edgar et al., 2007). The eruption impacted >600 km² of the island, emplacing an ignimbrite sheet up to 40 m thick, and culminated in caldera collapse within Las Cañadas. The Poris ignimbrite succession, comprising layers of lapilli tuff, lithic breccia, ash and pumice fall layers, is exposed and well documented in the Diego Hernandez wall (N. Smith & Kokelaar, 2013) and across the Bandas del Sur (Edgar et al., 2002; Brown & Branney, 2004b, 2013).

146

147

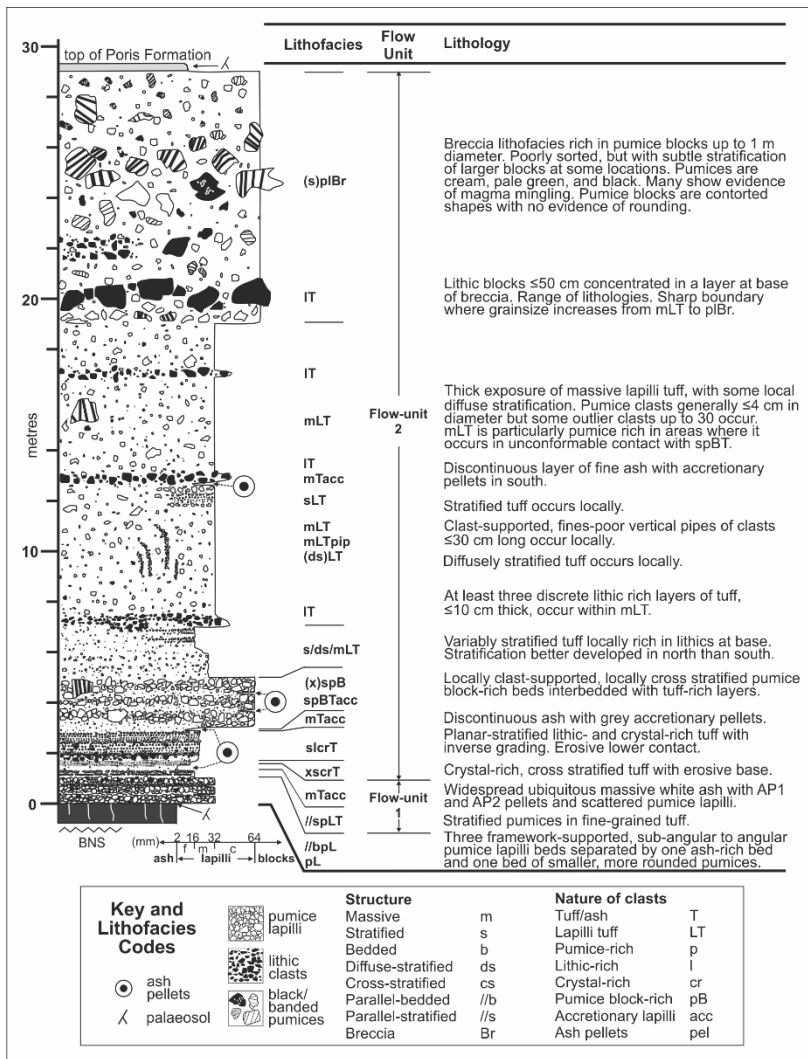
148

149

150

151

Work by Smith and Kokelaar (2013) and Brown and Branney (2004b) applies the same lithofacies architectural approach to the analysis of proximal and distal Poris deposits (respectively; summarised in figures 3 and 4). The studies report different proximal and distal lithofacies, with apparently contradictory records of hiatus and therefore different numbers of flow units. There are no reported medial exposures to connect these distinct proximal and distal records, therefore the Poris provides a novel opportunity to examine lithofacies and flow unit correlation for a major Plinian eruption event and consider its implications.



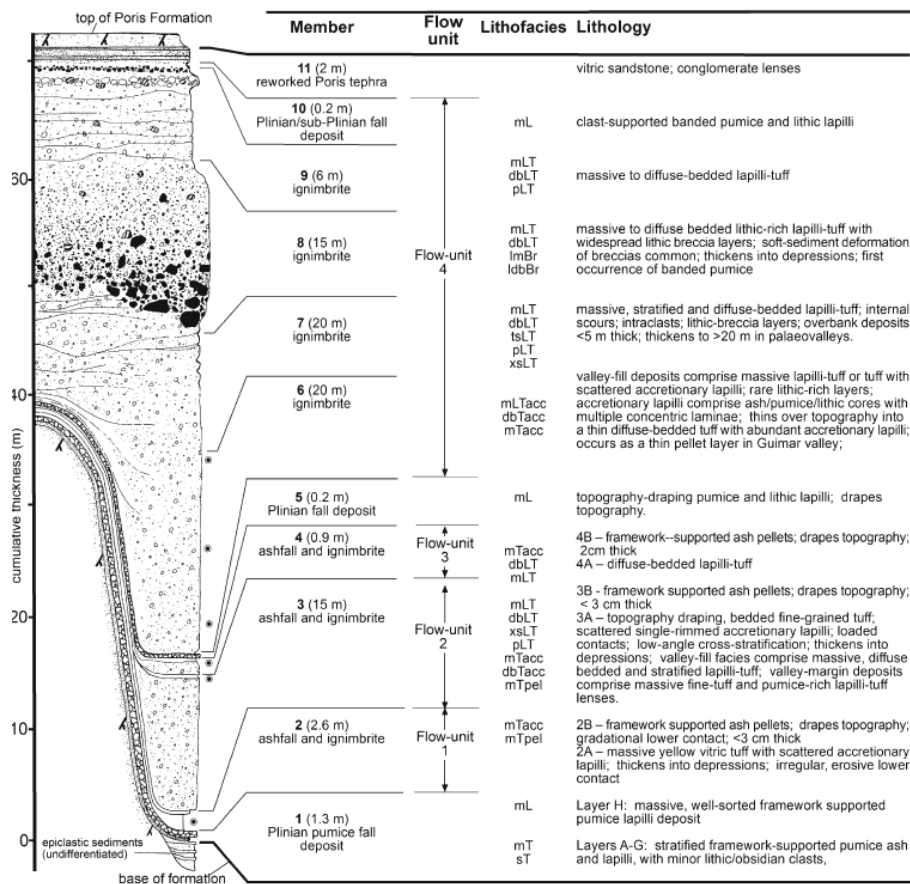
152

153

154

155

Figure 3. General vertical section of the proximal Poris ignimbrite succession (reproduced from Smith and Kokelaar, 2013). Legend is relevant for all logs presented within this work. For full description of lithocodes, see Brown and Branney (2004b).



156

157

158

Figure 4: General vertical section of the distal Poris ignimbrite succession (reproduced from Brown and Branney, 2013). Note difference in vertical scale between Figures 3 and 4. For legend, see Figure 3.

159

160

161 3. Methodology

162

3.1 Stratigraphic analysis

163

164

165

166

167

This study provides a new correlation of proximal (detailed in Smith & Kokelaar, 2013) and distal (detailed in Brown & Branney, 2004b, 2013; Edgar et al., 2002) sequences of Poris pyroclastic stratigraphic architecture, through entrachron analysis, comparison of lithofacies and evidence of hiatus. In the Poris succession, the occurrence of Plinian units and co-ignimbrite ash fall layers are evidence of cessation in PDC activity, while entrachrons include the appearance of pumice and lithic clasts with distinctive colours and compositions.

169 The term ‘lithofacies’ is used within this study to refer to a part of an ignimbrite that has distinct physical
170 characteristics (after Branney and Kokelaar, 2002). ‘Architecture’ is the overall structure of the ignimbrite and how
171 the lithofacies are arranged. Each non-genetic lithofacies name is attributed based upon these characteristics (see
172 Figs 3 and 4). The term ignimbrite ‘vener’ is used as a non-genetic description for thin ignimbrite deposits on
173 topographic highs. The grain-size system used on stratigraphic logs is that developed by Cas et al., (2008) for
174 volcanic nomenclature. The terms “proximal” and “distal” denote the present Diego Hernandez caldera sector
175 (likely within 4 km of the original Poris vent) and the Bandas del Sur coastal zone respectively. Ash aggregates
176 within ignimbrite stratigraphy are characterised using the framework provided in Brown et al. (2012); AP1
177 aggregates are poorly constructed, fragile ash pellets, whereas AP2 are subspherical accretionary pellets typically
178 with an ash core surrounded by a rim of multiple concentric laminae.

179 **3.2 Geochemical analysis**

180 A small-scale analytical study of Poris pumices from the Diego Hernandez wall and the coastal Bandas del Sur
181 zone was undertaken as part of this study to verify stratigraphic correlation and confirm that proximal and distal
182 successions studied are indeed counterparts. Pumice sampling was carried out during NJD’s PhD thesis (N. Smith,
183 2012) in 2009, and samples were geochemically analysed using X-Ray Fluorescence and Electron Microprobe
184 analysis facilities at Leicester University in 2010. XRF was chosen in preference to single-grain tephra analysis
185 methods to allow data to be compared with previous XRF studies of Tenerife ignimbrites (Brown, 2001; Edgar et
186 al., 2002). Proximal Diego Hernandez samples were collected from the Cerrillar Gully and log locations 5, 10, 11,
187 13, 16 and 17 of Smith and Kokelaar (2013). Distal Bandas del Sur samples were collected from the Poris Quarry,
188 Güimar Road, Tajao Road and Spooky Dog locations reported in Brown (2001), Brown et al. (2003) and Brown
189 and Branney (2004b). Pumice samples were predominantly cream in colour, but also included black, green and
190 mingled types. A full sample list and analytical methods can be found in Supplementary Material.

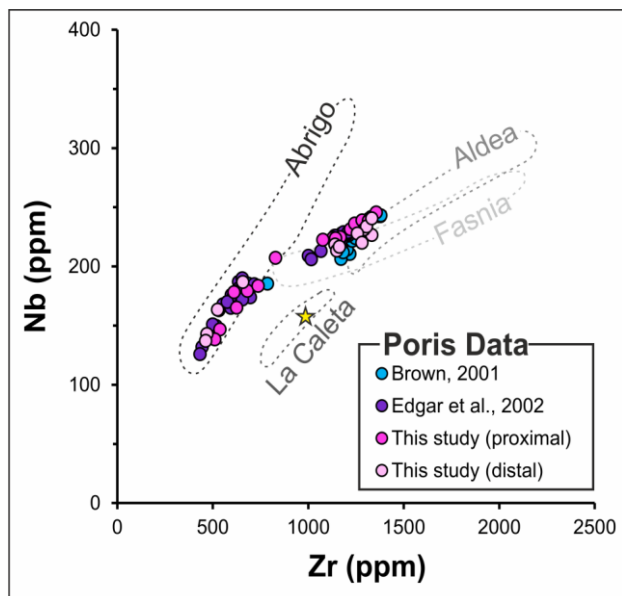
191

192 **4. Proof of Poris**

193 Stratigraphic and geochemical evidence confirms that proximal and distal exposures correlated in this study are
194 counterparts of the Poris eruption. These outcrops have been put in stratigraphic context by previous studies
195 (Brown et al., 2003; Edgar et al., 2007), and have been geochemically analysed by Brown (2001), Edgar et al.,
196 (2002) and others (e.g. Edgar et al., 2007). When existing data are plotted together with the new data from this

197 study on a Zr-Nb covariation plot, proximal and distal samples show clear overlap (see Fig. 5). Furthermore, an
198 ignimbrite overlying a paleosol on top of proximal Poris deposits sampled during this work was found to be a
199 geochemical match to the 221 ka La Caleta ignimbrite (based on data fields from Edgar et al., 2007; see Fig. 5).
200 The La Caleta eruption followed the 273 ka Poris event (Brown et al. 2003).

201



202

203 **Figure 5: Geochemical correlation showing Poris data from this study and two previous geochemical studies (Brown,**
204 **2001 and Edgar et al., 2002). Stippled outlines show data fields for other ignimbrite formations of the Diego**
205 **Hernandez episode of Tenerife volcanism for comparison (from Edgar et al., 2002). Star marks composition of**
206 **proximal La Caleta sample. Note the two distinct data fields of the Poris eruption, highlighting the bimodal**
207 **composition with more felsic and mafic compositions.**

208

209 5. Using entrachron analysis to correlate contradictory eruption history

210 In this section physical characteristics of proximal and distal Poris deposits are summarised (detailed observations
211 and interpretations are within Smith and Kokelaar (2013) and Brown and Branney (2004b, 2013) respectively) and
212 a new stratigraphic correlation and reconciled interpretation is presented (see Table 1). Descriptions of distal Poris
213 stratigraphy by Edgar et al. (2002) using a different lithofacies system are not covered in detail below, but have
214 been considered and are reconciled with correlations presented here in Table 1. For ease of reading, interpretations
215 are presented alongside correlations, and discussed more fully in the next section.

216

217 In this work, we interpret flow units by evidence of hiatus rather than by changes in grading or bedding patterns.
218 Where present, diffuse bedding, grading and discontinuous scour are interpreted as evidence of progressive
219 aggradation from a sustained PDC that experienced changing conditions at the flow boundary zone, rather than
220 evidence of multiple PDC events (Branney and Kokelaar, 2002). However, evidence from the Poris succession
221 illustrates how such changes at the flow boundary zone through time (unsteadiness) and in space (nonuniformity)
222 can be *linked* to PDC runout distance and hiatus, which we consider further in the Discussion.

223 **5.1 Phase 1: Plinian activity and ash fall (entrachon A)**

224 *Proximal record*

225 A parallel-bedded pumice lapilli facies overlies pre-Poris lavas across the proximal Diego Hernandez wall, ranging
226 from 10 cm – 1 m in thickness. Three layers of angular, framework-supported pumice lapilli occur separated by an
227 ash bed and a bed of rounded, smaller pumices. The unit contains abundant dark green obsidian fragments.

228 *Distal record*

229 The distal Plinian deposit consists of distinct beds of framework-supported pumice (B, D, E, G and H) interspersed
230 with ash layers (A, C and F). The pumice beds have different geographic distributions; lower beds (B, D, E) are
231 exposed between Fasnía and Aldea Blanca. Bed H is notably coarser and is thickest at Güimar in the east. Green
232 obsidian chips are markedly concentrated at the base of an exposure near Tajao.

233 *Correlation*

234 Distinctive green obsidian chips are found in both proximal and distal bedded Plinian material and form the first
235 correlative entrachron of the Poris succession, indicating that both proximal and distal material was created during
236 the same phase of Plinian activity (Fig. 6).

237

238 These lithofacies are similar in proximal and distal zones, with ash layers recognised between fallout layers distally,
239 and finer beds also interspersed in proximal fallout facies. However, they are not exactly equivalent and may not
240 be temporal correlatives.

241

Phase	Proximal record summary ¹	Distal record correlatives ^{2,3,4}	Entrachrons and rationale for correlation
8. Cessation of PDC activity and fallout	Plinian fallout is not recorded proximally; pumice-rich gravels and soil overlay the stratified pumice block breccia.	Member 10 Plinian/sub-Plinian fall deposit ² [Uppermost part of Guimar Member ³ ; Units F and G ⁴]. Overlain by reworked material.	Distal fallout has no proximal counterpart, although may temporarily correlate with upper parts of stratified pumice block breccia.
7. Waning PDC activity	Stratified pumice block breccia rich in black and banded pumices.	Member 9 ignimbrite ² [Guimar ³ ; Mareta ⁴]	Characteristics of both proximal and distal lithofacies are interpreted to indicate waning processes.
6. Peak intensity and caldera collapse	Lithic block layer and increased occurrence of black, green and banded pumice. Matrix colour change from cream to pinkish beige.	Member 8 lithic-rich ignimbrite, with first distal occurrence of black and banded pumices ² [Tamadaya ³ ; Quinta ⁴]	Entrachron D: Increased lithic block entrachron. Entrachron E: Black and banded pumice entrachron. Pink matrix colour noted in both proximal and distal facies.
5. Unsteady waxing PDC activity with scour and bypass	Stratified to diffusely-stratified tuff overlain by massive lapilli tuff containing distinct lithic-rich layers.	Members 6 and 7 ignimbrite ² [Rio and underlying Jurado ³ ; Upper part of Abona ⁴].	Proximal stratified facies are interpreted as deposits of a non-uniform, unsteady current, as is the Jurado ³ . Upper part of Abona ⁴ reported to contain subunits bounded by lithic breccia layers, similar to proximal facies. Evidence of scour and bypass occurs in both proximal and distal lithofacies.
<i>DISTAL PDC HIATUS</i>			
4. Simultaneous Plinian and PDC activity, with period of distal PDC hiatus	Locally framework-supported, cross stratified pumice block facies containing AP2 accretionary pellets and green pumices.	Member 4 ashfall and ignimbrite ² , Member 5 Plinian fall deposit ² [Cueva Honda ignimbrite, Caballos fallout ³ ; Unit D fallout overlain by Unit E 'surge' ⁴]	Entrachron C: Pale green pumices. Proximal facies is a unique to proximal area, exhibiting evidence of deposition by both fall and flow processes ⁶ . Distinct pale green pumices occur in both proximal facies and distal fallout.
<i>DISTAL PDC HIATUS</i>			
3. Phreatomagmatism and renewed PDC activity, with period of distal PDC hiatus	Cross stratified fine grained tuff overlain by distinctly grey crystal-rich planar stratified tuff. Discontinuous ash layer with grey accretionary pellets.	Member 3 ashfall and ignimbrite ² [Magua ³ ; Manteca ⁴]	Entrachron B: Grey accretionary pellets. The grey cross- and planar-stratified tuff facies are uniquely proximal, but both proximal and distal correlatives are grey in colour, with distinctive grey accretionary pellets.
<i>WIDESPREAD PDC HIATUS</i>			
2. First density stratified PDC, followed by widespread PDC hiatus	Stratified pumices within tuff overlain by continuous, massive ash-rich tuff	Member 2 ashfall and ignimbrite ² [Centinela ³ ; Unit C 'surge' ⁴]	Both proximal and distal units overlie the Plinian deposit below with no evidence of a time break. AP2 ⁵ accretionary pellets occur in both the Centinela and proximal massive ash facies.
1. Plinian activity with ash deposition	Parallel bedded pumice lapilli facies overlying pre-Poris lavas	Member 1 Plinian fall deposit ² [Hidalga ³ ; Unit B fallout ⁴ ; Unit A ash ⁴]	Entrachron A: Green obsidian. Green obsidian fragments occur in proximal and distal fallout. Lithofacies are physically similar in proximal and distal zones.

242

243

244

245

Table 1: Summary of the stratigraphic correlation between proximal and distal Poris lithofacies presented in this paper. Superscript indicates references (1: Smith and Kokelaar, 2013; 2: Brown and Branney, 2013; 3: Brown and Branney, 2004b; 4: Edgar et al. 2002; 5: Brown and Branney, 2012; 6: Dowey and Williams, 2022).

246

247

248

249 *Interpretation*

250 The Poris eruption began with formation of a dilute ash cloud, deposition from which is recorded in the southeast
251 of the island. A Plinian plume developed and pumice deposition commenced, along with lithic material derived
252 from an obsidian-rich vent zone. The concentration of obsidian chips at the base of the deposit at Tajao could reflect
253 subtle differences in terminal fall velocity between pumice and lithic clasts.

254

255 The deposition of ash records temporary hiatus in Plinian activity, which may reflect unsteadiness in the Plinian
256 column at source, and/or may have been localised due to changes in wind direction. A subrounded pumice bed in
257 the proximal zone indicates dilute pyroclastic current activity or wind action, at least proximally, sufficient to
258 rework Plinian material. The distal record indicates that Plinian dispersal gradually shifted from southeasterly to
259 easterly. There is no proximal physical equivalent of the coarser pumice facies observed at Güimar, although the
260 upper part of the proximal Plinian unit is interpreted to have been reworked during phase 2 (see below), therefore
261 any equivalent material may have been removed.

262



263

264 **Figure 6. Dark green obsidian lithics are abundant in proximal and distal exposures of Poris Plinian fallout. Photo**
265 **taken at location in the DH caldera wall at 28.280273°N, 16.549526°W**

266

267 **5.2 Phase 2: First density stratified PDC activity and widespread hiatus**

268 *Proximal record*

269 Stratified layers of Plinian-population pumices, and smaller, rounded pumices, within tuff are in erosional contact
270 with the Plinian deposit. This facies is overlain by a continuous, massive ash-rich tuff, <200 mm thick, containing

271 both AP1 unstructured ash pellets and AP2 accretionary pellets ≤ 20 mm in an ash-rich matrix with scattered
272 subangular Plinian-population pumice lapilli.

273 *Distal record*

274 A massive, fine-grained vitric tuff containing AP2 accretionary lapilli and Plinian population pumices occurs above
275 the distal Plinian unit. This tuff has an erosive lower contact and thickens into depressions, and is overlain by a
276 layer of framework supported AP1 pellets (≤ 15 mm in diameter) that drapes topography.

277 *Correlation*

278 Both proximal and distal lithofacies in this part of the succession record the onset of PDC activity, but have different
279 characteristics. Distally there are no stratified pumice lithofacies. Proximally there are no framework-supported
280 pellet facies. Correlation is inferred through location-based interpretation of these lithofacies.

281 *Interpretation*

282 A pyroclastic density current was generated by fountaining of the eruption column following widening of the
283 obsidian-rich vent. At first, only dilute upper parts were able to surmount the caldera topography in the DH sector
284 of the proximal zone, where it was able to roll, saltate and rework Plinian pumice lapilli from the underlying
285 substrate to create stratified layers of pumice within tuff (Fig. 7). However, where this density-stratified PDC was
286 able to reach the coastal zone, potentially coevally through topographic lows in the wall, it deposited valley-fill tuff
287 in topographic lows and veneers on topographic highs. Multi-rimmed AP2 ash aggregates that formed in the density
288 current were deposited along with ignimbrite (Brown et al. 2010). This is the first of three valley fill and veneer
289 ignimbrites recognised in the distal Poris succession.

290

291 The widespread ash-aggregate-rich layer found both proximally and distally is interpreted to record a widespread
292 hiatus in PDC activity that allowed for deposition and preservation of unstructured ash pellets. Proximally, multi-
293 rimmed accretionary pellets became deposited along with unstructured ash pellets in an ash-laden near-plume
294 environment (see discussion). Distally, a layer of clast-supported AP1 pellets formed by fallout from the co-
295 ignimbrite cloud.

296

297

298

299 **Figure 7. Evidence of widespread hiatus is registered by massive ash facies with accretionary lapilli in the DH wall,**
300 **and widespread ash pellet layer distally.**

301 **5.3 Phase 3: Phreatomagmatism and PDC activity (entrachron B)**

302 *Proximal record*

303 Proximally, the aggregate-rich ash is overlain by a thin cross-stratified, fine-grained tuff with an erosive base,
304 which is overlain and scoured into by a distinctly grey, stratified tuff rich in small crystals and altered lithics
305 (including plutonics), with variable stacked layers of inversely graded pumices. In two northern exposures this
306 facies is capped by an ash layer containing distinctive small accretionary pellets (<1 cm) with grey cores and less
307 brittle rims than in the facies below. In central and southern exposures the grey lithic- and crystal-rich stratified
308 unit has a gradational contact with the facies above and the pellet layer is absent.

309 *Distal record*

310 In the distal stratigraphic sequence, the phase 2 ash pellet layer is overlain by a second valley fill and veneer
311 ignimbrite; a grey, massive, AP2 accretionary lapilli-bearing tuff that thickens in depressions and shows complete
312 gradation to veneer facies on steep slopes and paleohighs. This is capped by a second thin AP1 ash pellet layer that
313 is extensive across the distal region. A third veneer and valley-fill ignimbrite overlies this, outcropping between La
314 Caleta and Montana Magua, capped by a third AP1 ash pellet layer. In this facies, ash pellets exhibit distinct grey
315 cores.

316 *Correlation*

317 The lithic-rich, grey, cross stratified and planar stratified tuff facies are uniquely proximal lithofacies; no reported
318 distal lithofacies is rich in fine lithics or similarly stratified. However, the grey colour of the distal massive lapilli
319 tuff is an indication that it may be a distal counterpart. The small, grey accretionary pellets observed proximally
320 and distally (Fig 8) are interpreted here as a distinctive entrachron and are the basis for correlation of these facies.

321 *Interpretation*

322 Very fine fragmentation of lithics in the proximal facies is interpreted here as a proximal record of heightened
323 explosivity, recording a period of phreatomagmatism. This unit has characteristics similar to phreatomagmatic
324 ignimbrites at Somma-Vesuvius, and contains altered plutonics that may indicate a period of interaction with a
325 hydrothermal system at depth (Barberi et al., 1989; Cioni et al., 1999).

326

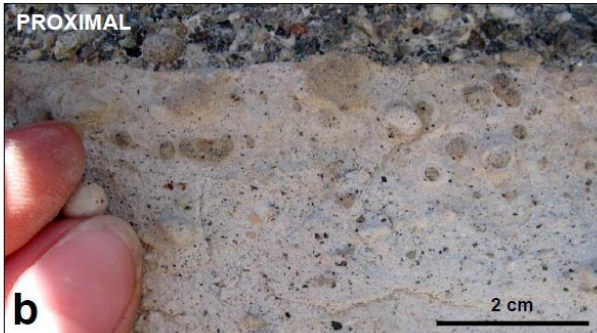
327 Lithic material from the conduit and vent zone became finely fragmented and entered a pyroclastic density current.
328 PDC activity was at first energetic and erosive, and potentially led to bypass to distal zones. In the proximal region,
329 the PDC was rich in fine lithics, creating distinct lithofacies, but by the time it reached the distal flanks it had shed
330 much of its lithic load and deposited more typical massive lapilli tuff. On distal topographic highs between
331 barrancos, ignimbrite veneer was deposited.

332

333 Unsteady waning of PDC activity then occurred, recorded in stacks of stratified and graded pumices (Fig. 9)
334 proximally. Local hiatus at the northern edge of the Diego Hernandez paleovalley allowed ash pellets to be locally
335 deposited while deposition continued elsewhere along the wall. Unsteady waning led to changes in PDC run-out
336 distance and episodes of distal hiatus, during which deposition of ash pellets from a co-ignimbrite cloud occurred.

337

338 Phreatomagmatism may have contributed to the different style of ash aggregate observed during phase 3. Highly
339 fragmented fine-grained lithic material entered the plume as a grey ash, and ash aggregates containing grey ash
340 cores formed. The irregular, contorted nature of the accretionary pellets at this stage, compared to those elsewhere
341 in proximal stratigraphy, may indicate that the pellets underwent less 'baking' within the plume and/or PDC.
342 Conceivably, phreatomagmatic conditions may have caused a drop in temperature of the erupted material,
343 contributing to this effect.



344
345
346

Figure 8: The grey ash pellet entrachron, evidenced in both the proximal (28.280273°N, 16.549526°W) and distal (Tajao Road locality) region.



347
348
349

Figure 9: Repeating stacks of inversely graded pumices deposited during episode of PDC waning in the proximal zone 28.280273°N, 16.549526°W

350

351 **5.4. Phase 4: Simultaneous Plinian and PDC activity (entrachron C)**

352 *Proximal record*

353 A locally framework-supported, cross stratified pumice-block facies containing AP2 accretionary pellets overlies
354 the grey lithic stratified facies in the DH wall. Pumice blocks up to 300 mm diameter occur and contain mafic
355 blebs. Larger pumices are distinctly pale green in colour. Fines-rich layers separate pumice-rich beds, with evidence
356 of internal scour. Low-angle cross-stratification occurs and pumice beds pinch out across exposures. AP2
357 accretionary pellets occur and are brittle, relatively large (<20 mm), with white cores.

358 *Distal record*

359 The third distal ash pellet layer is stratigraphically overlain by a topography-draping layer of framework-supported
360 pale green pumice lapilli. It occurs between La Caleta and El Baul and approaches 120 mm thick in Güimar, but is
361 only one clast thick southwest of Poris de Abona. This is the second Plinian fallout unit recorded distally.

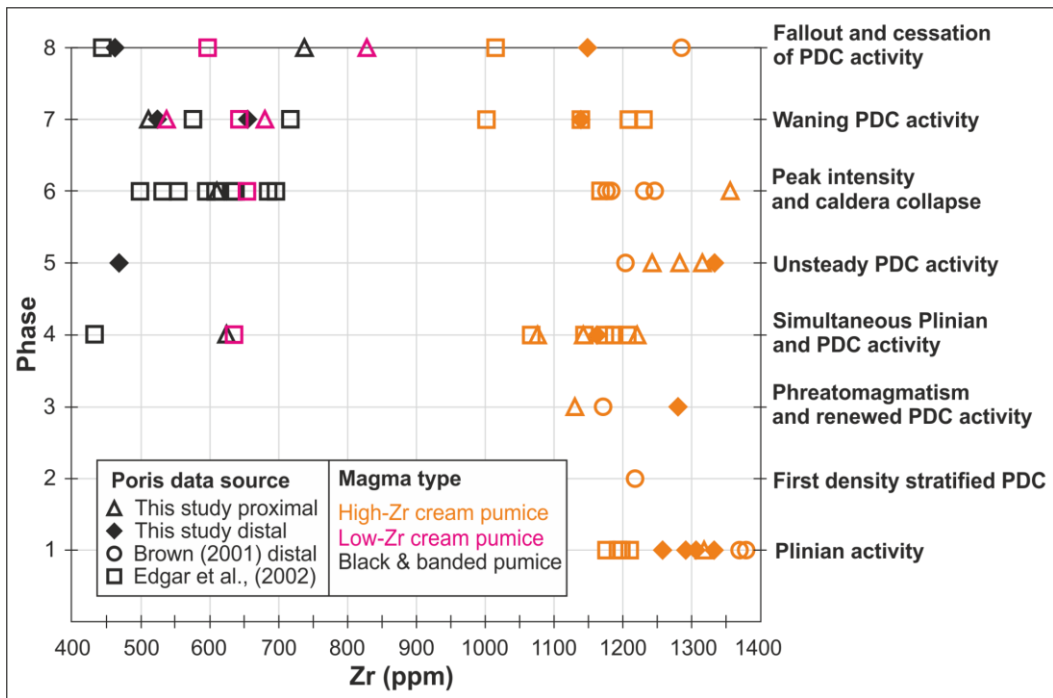
362 *Correlation*

363 The proximal cross stratified pumice block lithofacies is another exclusively proximal lithofacies. It exhibits
364 evidence of deposition by both fallout and flow processes (Dowey & Williams, 2022), and contains zones of
365 angular, framework-supported pumices that share characteristics with the distal Plinian unit. The distinct pale green
366 pumices present in both the proximal pumice block unit and the distal Plinian unit are interpreted here as a
367 correlative entrachron.

368

369 Pumice samples from this stage of the eruption (taken from the proximal cross stratified pumice block lithofacies
370 and distal second Plinian facies) both contain notably less Zr than proximal and distal samples of the initial opening
371 Plinian event (~1200 ppm on average as opposed to ~1400 ppm respectively) (Fig 10).

372



373

374 **Figure 10: Zirconium concentration plotted against interpreted phase for Poris data from this study, Brown (2001)**
 375 **and Edgar et al., (2002). Using nomenclature and correlations summarised in Table 1, data plotted at each phase are:**
 376 **1 = //bpL (this study), Unit B (Edgar), Hidalga (this study; Brown); 2 = Centinela (Brown); 3 = slcrT (this study), Magua**
 377 **(this study; Brown); 4 = spBT (this study), Abona (Edgar), Caballos (Brown); 5 = s-ds-mILT (this study), mLT (this study),**
 378 **Jurado (Brown), Rio (this study); 6 = base of splBr (this study), Tamadaya lBr (Brown), Quinta (Edgar); 7 = splBr (this**
 379 **study), Tamadaya [above lBr] (this study), Mareta (Edgar); 8 = top contact of splBr (this study), Guimar (this study;**
 380 **Brown), Units F and G (Edgar). Note that at phase 8, waning stage fallout is the uppermost distal Poris deposit.**
 381 **Proximally, there is no upper fallout recorded, therefore pumice analyses from the uppermost part of splBr are**
 382 **plotted here for comparison.**

383 *Interpretation*

384 Following the phreatomagmatic phase, the eruption reverted to magmatic and a Plinian column significant enough
 385 to be recognised in the rock record was established. Proximally, PDC activity did not cease and proximal coarse
 386 Plinian fallout interacted with turbulent density currents to form a novel hybrid lithofacies (Dowey & Williams,
 387 2022). The hiatus in PDC activity across the distal region (that had allowed for deposition of the third ash pellet
 388 layer) now allowed for Plinian deposition to be recorded in the Bandas del Sur. The proximal hybrid lithofacies is
 389 therefore a time correlative to the distal Plinian unit, and possibly also to parts of overlying distal ignimbrite facies.

390

391 There is no evidence of hiatus in PDC activity in the proximal area at this time, but there is evidence that proximal
392 density current activity was unsteady and non-uniform; stratification and fine-grained ash and crystal layers
393 deposited between pumice block rich beds reflect changing conditions at the flow boundary zone.

394

395 The influx of pale green pumice and lower Zr bulk pumice chemistry at this stage may reflect the tapping of a
396 different zone of the magma system during and following phreatomagmatism. A subtle change in plumbing may
397 also account for the increased abundance of mafic blebs observed in proximal pumices at this stage.

398 **5.5 Phase 5: Unsteady waxing PDC activity with scour and bypass**

399 *Proximal record*

400 The proximal hybrid unit is overlain by up to 2 m of variably stratified to diffusely stratified tuff, preserved at only
401 a few localities due to the erosive base of a more lithic-rich tuff facies above. In northern exposures this facies is
402 in sharp contact with the hybrid facies, and contains inversely graded pumices. In central exposures it is in
403 gradational contact with the hybrid facies below, and in southern Diego Hernandez outcrops it is in erosive contact
404 with the hybrid facies, truncating the pumice-block beds.

405

406 Stratigraphically above, and in erosive contact with, the stratified tuff lies 10-12 m of predominantly massive lapilli
407 tuff, containing distinct layers of lithic-rich tuff < 200 mm thick. These lithic-rich layers can be traced along the
408 Diego Hernandez wall and are associated with load and flame structures and scour and bypass surfaces. At one
409 location, the most southerly in the DH wall, a localised and discontinuous stratified ash layer, <50 mm thick, occurs,
410 overlain by a lithic tuff layer. The overlying lithic-rich layer can be traced across adjacent outcrops, but the ash
411 layer does not continue.

412 *Distal record*

413 A geographically-restricted valley fill ignimbrite overlies the second distal Plinian unit, consisting of massive lapilli
414 tuff that passes into thin ignimbrite veneers. This unit occurs between La Caleta and Güimar and comprises massive
415 lapilli tuff rich in accretionary lapilli that passes laterally into diffuse stratified veneers on paleohighs; at Güimar it
416 is associated with an ash pellet fall layer.

417

418 This lithofacies is overlain by a far more geographically extensive member, which in paleovalleys comprises
419 homogenous massive tuff up to 20 m thick. On paleohighs, a clear erosive surface occurs at its base. Veneer
420 exposures include variably stratified and cross stratified tuff, with layers of lithic lapilli and blocks common. This
421 part of the distal stratigraphy contains complex bedforms (Brown & Branney, 2004a), scours, and splay and fade
422 stratification.

423 *Correlation*

424 The proximal stratified to diffuse stratified tuff facies is vertically and laterally variable, indicating that this phase
425 began with turbulent, unsteady, non-uniform flow-boundary zone conditions (Branney and Kokelaar, 2002). The
426 geographically restricted distal veneer and valley fill ignimbrite may be its counterpart, although there is no clear
427 entrachron to connect the two. The widespread and thick nature of the more geographically extensive ignimbrite
428 makes this unit a likely counterpart of the proximal thick massive lapilli tuff lithofacies; both include zones of
429 lithic-rich tuff.

430 *Interpretation*

431 Sustained pyroclastic density current activity waxed in energy, but continued to be unsteady, with flow-boundary
432 zone conditions that led to stratified lithofacies proximally. Coarse proximal fallout input to the DH sector ceased
433 sufficiently to no longer be registered in the deposited material. PDC run out increased sufficiently to reach distal
434 zones, at first with a minimal geographic extent. The PDC did not reach Güimar but co-ignimbrite ash deposition
435 occurred at this location.

436

437 More significant pyroclastic density current waxing was likely then instigated by instabilities in the conduit-vent
438 region that led to increased entrainment of lithics into the current. Proximally, waxing is marked by erosion and
439 lithic-rich layers associated with scour. A highly localised ash bed at the southern edge of the DH wall is possibly
440 evidence of temporary thalweg migration within the DH paleovalley at this time (see discussion). Distally, waxing
441 is recorded in a sharp increase in the geographic extent of massive lapilli tuff at this time, with increasing lithic
442 content. The relatively small thickness of material recorded proximally at this stage indicates bypass of pyroclastic
443 material to the distal zone (where up to 30 m thickness of ignimbrite is recorded). Distally, regressive bedforms
444 indicate significant bypass into the sea (Brown & Branney, 2004a).

445 **5.6 Phase 6: Peak intensity and caldera collapse (entrachrons D and E)**

446 *Proximal record*

447 A lithic-block layer, <1.5 m thick, occurs in the Diego Hernandez wall. Matrix-supported blocks are up to 1 m in
448 diameter and include a wide variety of lithologies, including hydrothermally altered clasts (Fig. 11). This block
449 layer, just one or two blocks thick, occurs between the massive lapilli tuff below and a lithofacies rich in mafic
450 pumice blocks above. The contact with massive lapilli tuff is planar and distinct due to an increase in pumice size,
451 an increased occurrence of black, green and banded pumice, and a matrix colour change from cream to pinkish
452 beige.

453 *Distal record*

454 Distally, a massive to diffuse stratified lithic-rich lapilli tuff occurs, with widespread lithic breccia layers in tuff
455 with a pink-weathering matrix. This facies, which is up to 15 m thick, contains the first occurrence of mafic banded
456 pumices in the distal region. Load and flame structures involving underlying ignimbrite are common. This lithic-
457 rich facies has a gradational contact with overlying facies.

458 *Correlation*

459 The increased influx of lithic material and of mafic and banded pumices at this point in the eruption mark distinctive
460 entrachrons that enable correlation of this part of the distal sequence to the lithic block tuff layer in the DH wall
461

462 Cream pumices sampled from the matrix of the proximal lithic block layer and from the distal lithic-breccia
463 lithofacies have Zr contents ranging from 1150-1400 ppm. The black and banded pumices samples analysed from
464 these facies contain 500-800 ppm Zr (see Fig. 10).

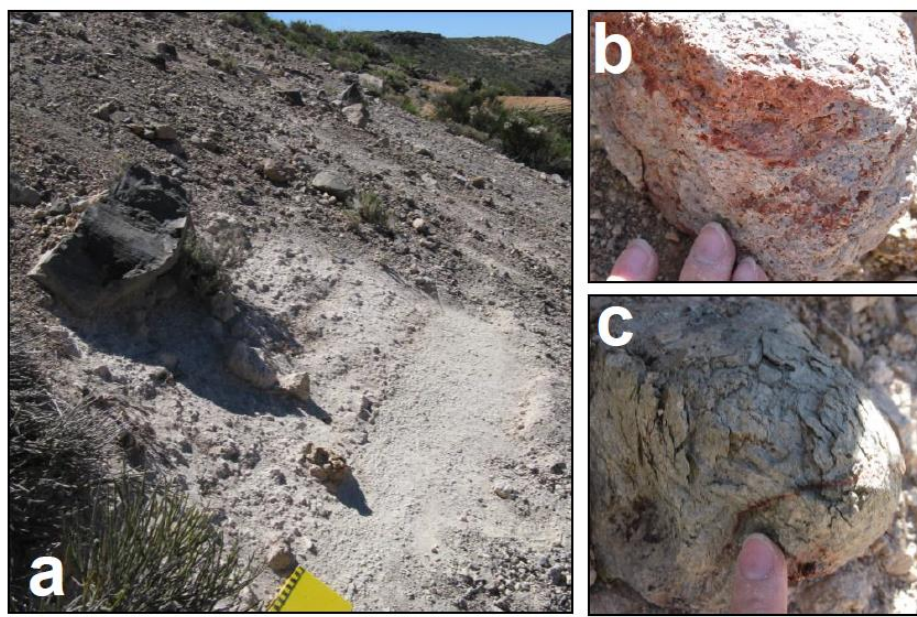
465 *Interpretation*

466 Following the ejection of large volumes of magma during phase 5 waxing PDC activity, a critical extent of magma
467 evacuation was reached. The 'chamber' roof collapsed, and large faults dilated, disrupting the surrounding
468 hydrothermal system. Conduit-derived, hydrothermally altered lithic blocks entered the unstable eruptive jet(s) and
469 the waxing pyroclastic density current became extremely lithic-rich.
470

471 The lower contact recording this phase is sharp in the proximal zone, whereas distally load and flame features are
472 common. This implies that the lithic-rich PDC was highly erosional in the near-vent zone, creating a relatively
473 planar surface, whereas distally material piled up on top of previously deposited 'fluffy' ignimbrite, and sank into
474 it. The thin proximal lithic-block layer implies significant bypass to the distal zone, where, relatively thick lithic
475 rich breccia is recorded.

476
477 Poris caldera collapse subtly changed the plumbing of a complicated internal system. Although available earlier in
478 the eruption, evident in blebs and mingled ballistics in proximal Phase 4 deposits, there was a large influx of the
479 low-Zr magma series in the closing stages of the Poris eruption. The contemporary eruption of two discrete (high-
480 Zr and low-Zr) magmas also occurred during the Aldea, Fasnía, Caleta and Abrigo events, also recorded in the
481 Diego Hernandez wall (Edgar et al., 2007). It has been suggested that the coexistence of two separate magma
482 reservoirs throughout this ~300 ka period is unlikely; the persistence of the distinct magmas may instead reflect
483 repeated melting of different protoliths, with repeated fractionation of the magmas, following the caldera collapse
484 and structural changes associated with each major eruption (Edgar et al., 2007).

485



486

487 **Figure 11. (a) The transition from massive lapilli tuff to the lithic block layer in the proximal Poris succession, visible**
488 **when scree is brush away. Large lithic boulder projecting at angle is 40 cm across and in situ. Hydrothermally altered**
489 **blocks (b) and lithics with spallation texture are observed (c).**

490 **5.7 Phase 7: Waning PDC activity**

491 *Proximal record*

492 A poorly-exposed, 10 m thick, stratified pumice-block breccia, rich in banded and black pumice blocks ≤ 1.5 m in
493 diameter, is present atop phase 6 massive lapilli tuff across the DH wall. A key exposure of this breccia occurs in
494 a gully at Montaña El Cerrillar just north of the DH wall. Lithic clast size is similar to that seen in the Poris massive
495 lapilli tuff. Stratification is variable and is distinguished by the changing abundance of pumice blocks; some zones
496 have greater concentrations of large pumices whereas others are richer in lithics.

497 *Distal record*

498 A massive, diffuse bedded and pumice-rich lapilli-tuff facies with a relatively low lithic content overlies the distal
499 lithic-rich breccias with a gradational contact. These facies contain both cream phonolitic and banded
500 tephriphonolitic pumice. The lower bed comprises a thin (200–400 mm), massive layer with abundant inverse-
501 graded pumices and normal-graded lithic lapilli in many locations. The upper part contains clast-supported, pumice-
502 rich ignimbrite. The facies is up to 10 m thick.

503 *Correlation*

504 Correlation here is based upon the nature of the lithofacies, which, although very different, both indicate waning
505 processes. Proximally, after considerable bypass during phase 6, deposition has begun again, with preservation of
506 large pumice blocks, indicating waning. Distally, normal grading of lithic clasts and inverse grading of pumices is
507 indicative of waning flow (Branney & Kokelaar, 2002).

508

509 The occurrence of large phonotephrite pumice blocks is striking in the proximal region, but the black/banded
510 pumice entrachron is placed where the influx of black/banded pumice material is first recorded (at the point of the
511 lithic block layer).

512 *Interpretation*

513 Following climactic explosions and caldera collapse, pyroclastic density current activity waned in energy enough
514 for at least 10 m of material containing large pumice clasts to be deposited proximally, although runout was still
515 sufficient to have widespread coverage of distal reaches. The similarity in thickness between the proximal and
516 distal waning stage facies at this stage may be coincidence (the thickness removed during post-Poris reworking is

517 unknown), but it could be an indication that aggradation was persistent in the proximal zone during this waning
518 phase with little bypass. The lack of coarse pumice blocks in distal exposures is most likely to be due to breakage
519 during transport across the volcanic flanks. As the PDC waned and run out distance decreased, retrogradation of
520 the ignimbrite sheet led to a strand line of pumice rich material in the upper part of the distal ignimbrite (Brown
521 and Branney, 2013).

522 **5.8 Phase 8: Cessation of PDC activity and fallout**

523 *Proximal record*

524 The stratified pumice-block breccia is the final deposit recorded proximally. In the DH wall, it is directly overlain
525 by a soil 38 cm thick, and in the Cerrillar Gully it is overlain by 5 m of stratified pumice-rich gravels.

526 *Distal Record*

527 At Güimar, the uppermost distal Poris ignimbrite lithofacies is overlain by a clast-supported lithofacies comprising
528 cream pumice lapilli overlain by banded pumice lapilli. This fallout unit is overlain by reworked Poris material.

529 *Correlation*

530 The distal fallout layer at Guimar has no proximal counterpart although it may temporally correlate with upper
531 parts of the proximal stratified pumice block unit.

532 *Interpretation*

533 Pyroclastic current activity ceased in the distal zone and Plinian fallout tephra was deposited, recorded at Güimar.
534 Plinian deposition may have been ongoing throughout the Poris eruption, only being recorded when currents waned
535 sufficiently (during phase 4). Alternatively, Plinian activity may have ceased following the hybrid phase and
536 restarted towards the end of the eruption. The lack of a proximal physical relative to the distal fallout layer
537 could be due to post-eruption sedimentary reworking, but it may reflect continuation of pyroclastic density current
538 activity in the proximal zone after flow had ceased in the distal zone. As the current waned, regressive deposition
539 of tuff may have occurred as the flow run-out distance diminished; Plinian pumices would have fallen into the
540 current in the proximal zone and would not have been recorded as a fallout layer.

541

542 **6. Synthesis**

543 **6.1 Correlating flow units to create a coherent narrative for the 273 ka Poris event**

544 The distal Poris ignimbrite succession records four flow units, delineated by three widespread ash pellet fallout
545 layers, providing evidence for four discrete pyroclastic density currents during the 273 ka Poris eruption. However,
546 the proximal record contains definitive evidence for only two flow units (delineated by the phase 2 ash lithofacies).
547 Only *local* hiatus in ignimbrite deposition is recorded subsequently in the proximal succession, in discontinuous
548 ash beds with ash aggregates at the northern (phase 3) and southern (phase 5) edges of the Diego Hernandez wall.
549 Entrachron analysis of the distal and proximal records indicates that many distal lithofacies have a temporal,
550 although not always physically similar, proximal counterpart lithofacies, allowing correlations to be made between
551 the two records and a coherent story to be developed. We propose that the documented Poris succession could have
552 been deposited by only two, density-stratified, pyroclastic currents (Fig. 12).

553
554 Following an opening phase of Plinian fallout activity (phase 1), an initial PDC was generated but was relatively
555 small, and was initially blocked by caldera topography proximally (phase 2). There was then a fundamental hiatus
556 in PDC activity across proximal and distal zones, allowing ash aggregates to be deposited proximally and the first
557 co-ignimbrite ash pellet layer to be deposited distally.

558
559 A second PDC was generated during a phase of phreatomagmatic activity. This second current was sustained, but
560 experienced unsteadiness through time. During periodic waning, deposition continued close to source but changes
561 in run out distance led to two widespread hiatuses in the distal zone: the first is recognised in an ash pellet fallout
562 layer and correlates with local hiatus proximally (phase 3); the second is recognised by an ash pellet fallout layer
563 and overlying Plinian unit, which correlates temporally with unsteady hybrid activity proximally (phase 4).

564
565 Current activity then began to step up (phase 5), with a transition from stratified to massive lapilli tuff facies
566 proximally, an incursion of lithic-rich layers, and an increasing geographic distribution of ignimbrite facies in distal
567 reaches with evidence of bypass to the sea. This episode, which likely coincides with incremental destabilisation
568 of the edifice, culminated in caldera collapse (phase 6) marked by a significant influx of both lithics and banded
569 pumices in proximal and distal reaches, and considerable bypass of the proximal area. Following this, PDC activity
570 began to wane, recorded in distinctly different lithofacies in proximal and distal zones (phases 7 and 8). During the
571 final waning stage of the eruption (phase 8), the run-out distance of the density current gradually decreased and
572 Plinian deposition was recorded in some distal zones.

573 **6.1 Potential for additional hiatus**

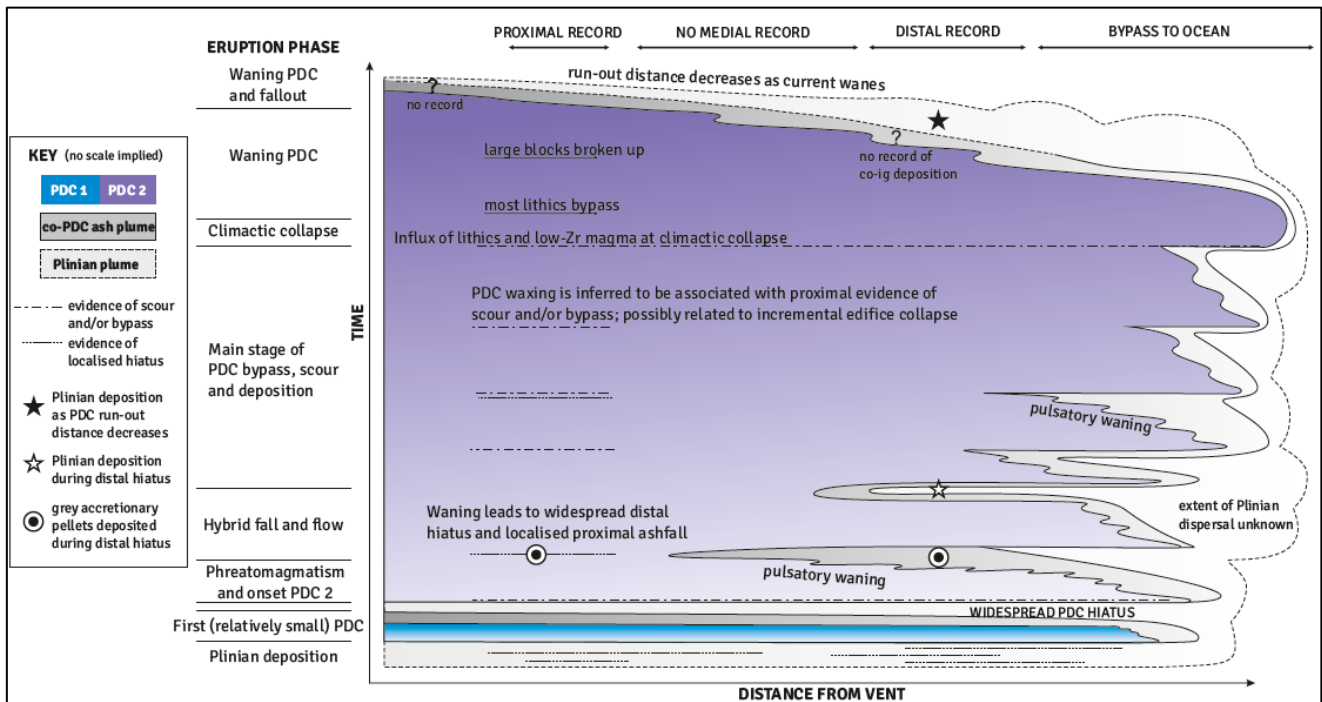
574 The potential that more hiatus episodes occurred during Poris PDC activity and were lost from the rock record by
575 cryptic erosion must be considered. It seems unlikely that further significant hiatus would have occurred during
576 phase 5 and 6, at a time when lithofacies indicate that PDC activity was waxing dramatically. If periodic
577 unsteadiness of the second, sustained PDC occurred at this time, run-out distance of the current at this point was
578 such that no further hiatuses would have been recorded in the Bandas del Sur. Although lithofacies from the earlier
579 phases of current activity were partly removed during phase 5 erosion (see log 13 of Smith and Kokelaar, 2013),
580 there are key exposures where gradational and non-erosive contacts between lithofacies (logs 1-5 of Smith and
581 Kokelaar, 2013) make the likelihood of further, cryptic, hiatus during phases 1-4 seem slim.

582 **6.2 Missing parts of the puzzle**

583 It is important to recognise that the proximal Poris lithofacies architecture provides a local snapshot, giving insight
584 into the processes occurring in a particular sector during the eruption. No other proximal Poris exposures have been
585 reported, but if they did exist they may display a different set of lithofacies. Changes in dispersal direction,
586 topography and substrate around the vent would likely contribute to complex variability in different sectors (e.g.,
587 Fierstein et al., 1997). Vent-radial and medial exposures of Poris deposits would add to the eruption history,
588 possibly shedding more light upon the hiatus issues; but these aspects of the story remain missing.

589
590 The distal region provides a far broader realm of exposure, but only provides a record of the material that was not
591 bypassed to the ocean. It has been suggested, based upon onshore ignimbrite deposits of eruptions from the last
592 600 ka, that density currents mainly moved towards the southeast of Tenerife from the central Cañadas zone (Edgar
593 et al., 2007). However, because material bypassed into the ocean in the Bandas del Sur region, where the coastal
594 slopes are the least steep on Tenerife, and because there are few or no deposits in steeper medial reaches above
595 Bandas del Sur where currents must have passed, it is conceivable that pyroclastic density currents moved in other
596 directions away from the vent, and that these are not registered in subaerial deposits because of erosion or non-
597 deposition (Brown and Branney, 2004b). It is also possible that Poris deposits elsewhere on the island have been
598 eroded or destroyed during subsequent structural events such as lateral collapse, giving a misleading view of PDC
599 flow direction (e.g., Dávila Harris et al., 2011).

600



601

602

603

Figure 12: Schematic illustrating how PDC waxing and waning during the Poris eruption led to a conflicting record of flow units in proximal and distal zones

604

605

7. Discussion

606

7.1 Unsteadiness: what drives variable run out and hiatus?

607

Unsteadiness in PDCs, where a parameter such as velocity fluctuates through time (*e.g.*, Kneller & Branney,

608

1995) can impact mobility and run-out distance but is poorly understood in dense, granular PDCs. Unsteadiness

609

can manifest in pulsatory behaviour, the devastating impact of which was observed in real time during the 2018

610

eruption of Fuego volcano, Guatemala, where a series of pulses of valley-confined PDCs led to more than 400

611

fatalities (*e.g.*, Charbonnier et al., 2023). Unsteadiness, current instabilities and pulsatory behaviour can be

612

interpreted from the stratigraphic record (*e.g.*, Pollock et al., 2019), and have been linked to fluctuating eruption

613

conditions at the vent (*e.g.*, Pittari et al., 2006; Báez et al., 2020). Unsteadiness generated by source conditions has

614

been directly connected to mobility; increasing eruptive mass flux during Plinian events has been linked to

615

increased run-out distance of pyroclastic density currents in both numerical modelling (*Bursik & Woods, 1996*)

616

and field studies (Williams et al., 2014). However, it is important to note that source conditions are not the only

617 driver of unsteadiness; experimental PDC modelling illustrates that poly-disperse dense granular currents are
618 inherently unsteady under fluidised conditions, with pulses forming spontaneously even when a steady initial
619 current is provided (Rowley et al., 2023 and references therein). Similar observations have been made in the
620 modelling of other sustained gravity currents (such as turbidity currents; Kostaschuk et al., 2018).

621
622 In the case of the Poris eruption, influxes of lithics at ≥ 5 points in the proximal Poris succession (finely fragmented
623 lithics during phase 3, at least three discrete lithic-rich pulses recorded in layers of tuff in phase 5, and the influx
624 of lithic breccias of phase 6) are interpreted here to record episodes of waxing PDC activity. Each of these lithic
625 episodes can be correlated with either resumption of PDC activity distally (increasing run out), stepping up of distal
626 PDC intensity, or increased geographic extent of PDCs in the distal region. In this case, the influx of lithics indicates
627 that instabilities at the vent are a likely driver for the waxing activity; waxing phase lithofacies during the second,
628 sustained PDCs are each associated with influxes of lithics and/or banded pumices, indicating incremental
629 destabilisation (and potentially, gradual expansion) of the edifice and inferring increased mass flux at source. These
630 findings are similar to evidence from the younger 188 ka Abrigo ignimbrite of Tenerife, which has also been found
631 to contain lithic block zones interpreted to result from pulses of vent-derived lithic debris attributed to the onset of
632 caldera collapse (Pittari et al., 2006).

633
634 Whereas waxing activity is here linked to source conditions, there are indicators that waning activity may have
635 involved episodes of spontaneous unsteadiness within the current. In this study, waning is recorded in proximal
636 stratified units that correlate with reductions in run-out distally: stacked beds of coarse-tail grading of pumices in
637 phase 3 proximal facies locally culminate in a discontinuous ash bed in the northern DH wall, marking local hiatus,
638 and are correlated with a widespread hiatus in the distal region (grey ash pellet entrachron). In phase 4, stratification
639 of the hybrid pumice block facies marks unsteady behaviour in the proximal zone and correlates to widespread
640 distal hiatus marked by the deposition of the second Plinian unit (pale green pumice entrachron). The unsteady
641 conditions recorded in the phase 3 repeated stacks of proximal inversely graded beds may have been caused by the
642 pulsatory passage of spontaneously developed roll waves, shock-like disturbances that travel faster than the
643 material in the flow (Balmforth & Mandre, 2004 and references therein). The pulsatory passage of roll waves is
644 believed to be a contributing factor in the development of regularly stacked and thin pumiceous layers at ignimbrites
645 elsewhere (e.g. Mount St. Helens July 22nd and August 7th 1980 deposits, and Santorini Minoan deposits, observed
646 by PBK). Such waves, or pulses, have been seen in debris-flow flume experiments (Johnson et al., 2012), and have

647 been observed to be directly involved in particle sorting processes and the development of reverse graded sets in
648 fluidised granular flow analogue experiments (Rowley et al., 2023).

649
650 It is as yet unclear whether such features of spontaneous unsteadiness in PDCs could be intrinsically linked to
651 waning regimes; they have been observed in both hopper release-style experiments that provide an insight into
652 waxing-then-waning single-pulse type currents (Johnson et al., 2012) and also in a fluidised flume able to capture
653 more sustained current behaviours; but not yet under controlled sustained waning conditions (Rowley et al., 2023).
654 The potential scale of such features in nature is also unclear. To create the widespread decrease in run-out recorded
655 in distal exposures at this time, it seems likely that larger-scale waning conditions at the vent may have been
656 occurring, potentially in tandem with spontaneous current perturbations that created the distinctive repeating
657 lithofacies.

658 **7.2 Nonuniformity: the cause of spatial changes in lithofacies**

659 While proximal to distal hiatus transitions reflect changes in runout distance due to unsteadiness through time,
660 vent-radial lateral transitions in lithofacies are interpreted to record nonuniformity in space (Branney and Kokelaar,
661 2002). The discontinuous ash layers preserved in the very northern (phase 3) and southern (phase 5) fringes of the
662 DH paleovalley are interpreted here to record nonuniform deposition with different drivers:

- 663
- 664 1. Reduced lateral extent: During episodes of waning activity and decreasing run out distance, it follows that
665 lateral geographic extent may also decrease. This scenario seems likely to have caused restricted deposition
666 of the proximal discontinuous ash layer in phase 3. The ash is associated with underlying graded facies
667 indicating waning, and correlates with hiatus in the distal record. We infer that as the current waned, PDC
668 activity no longer stretched across the entire DH wall and ash fallout occurred in the northern sector,
669 contemporaneous with continued PDC activity (recorded in gradational contacts between phase 3 and 4)
670 in the southern DH sector.
 - 671 2. Thalweg migration: The second discontinuous proximal ash layer (phase 5) occurs at the southernmost DH
672 outcrop, and is not associated with stratigraphic evidence of waning. Elsewhere, deposition of massive and
673 lithic-rich layers of lapilli tuff records waxing PDC activity. The thalweg, the axis of flow and locus of
674 deposition of a density-stratified current, may meander across a plain during periods of sustained
675 aggradation from a PDC (e.g., Branney & Kokelaar, 1992; Watkins et al., 2002); it is possible that this

676 discontinuous ash layer may reflect temporary thalweg migration, rather than waning, which allowed ash
677 to locally be deposited and preserved.

678 **7.3 The influence of topography**

679 Topographic changes have been shown to have a significant impact on deposition from pyroclastic density currents,
680 for example by controlling locations of deposition (Branney & Kokelaar, 1997), influencing run out (Andrews &
681 Manga, 2011), impacting sedimentation from the flow boundary zone (Doronzo et al., 2010) and channelising flow
682 (Aravena & Roche, 2022). Topography may have a crucial influence on pulsatory and unsteady PDC behaviours -
683 recent numerical modelling has shown that interactions between granular PDCs and topography can induce
684 unsteadiness (E. Breard, pers. comm.). The impact of topography on PDCs, particular on dense granular PDCs, is
685 not fully understood and requires further analogue and numerical modelling. However, the correlative work
686 presented here shows that distinct topographic environments can lead to distinct deposition from the flow boundary
687 zone at the same point in time in proximal and distal exposures; potentially contributing to contradictory records
688 of eruption history in different locations. This builds upon previous work from other Quaternary ignimbrite sheets
689 on Tenerife highlighting complex associations between paleotopography and unsteady PDC behaviours (Pittari et
690 al., 2006).

691
692 During the Poris eruption, both caldera wall-scale and smaller-scale topographic obstacles across the Tenerife
693 landscape caused local unsteadiness and lateral non-uniformity in PDC dynamics, during both waxing and waning
694 phases of PDC activity. These impacts would have been dynamic; topographic variations and changes in substrate
695 as a result of scour and infill were ongoing during the eruption both proximally and distally, at a range of scales.

696
697 For example, proximally, caldera topography acted as a barrier to flow in front of the Diego Hernandez site in the
698 early stages of the Poris eruption. The Diego Hernandez paleovalley was part of pre-existing caldera topography
699 that caused the first density current generated to be recorded in the DH wall merely as a thin veneer; the parts of
700 the first current that surmounted it were fully dilute, turbulent and with traction at the base. Contemporaneously,
701 parts of the current that reached the distal region were experiencing different conditions at the flow boundary zone,
702 due to different topographic conditions. The presence of barrancos, ridges and topographic obstacles similar to
703 Tenerife's present-day landscape led to the development of ignimbrite valley-fill and veneer lithofacies associations
704 with complex internal architecture even in the earliest PDC deposits recorded in the distal zone (described in detail
705 in Brown and Branney, 2004b and 2013).

706 **7.4 The impact of proximity to the vent on ash deposition**

707 Deposits proximal to the vent during Plinian eruptions are known to exhibit complex stratigraphy due to the varied
708 processes acting in this zone (e.g., Houghton et al., 2004), but are often lost due to caldera collapse and subsequent
709 near-vent erosion. The Poris succession is rare in having exposed proximal and distal counterparts, and - although
710 apparently not as close to the Poris edifice as deposits in the Guajara sector of the wall were to their source
711 (evidenced in welded units and conduit-infill material, see Soriano et al., 2006) - the proximal DH succession
712 contains unique lithofacies, recording phreatomagmatism and hybrid processes not observed in the distal record
713 (Smith and Kokelaar, 2013; Dowey and Williams, 2022). Particularly relevant to this study is evidence that
714 proximity to the vent impacted the record of ash aggregates, key indicators of hiatus in the Poris record.

715
716 Distally, the PDC was the main source of ash during the Poris eruption. In the distal region, facies associations of
717 topography-filling ignimbrite containing multi-rimmed AP2 accretionary lapilli, overlain by widespread layers of
718 framework-supported AP1 ash pellets, are evidence of deposition by density-stratified PDCs followed by hiatus in
719 PDC activity. The AP1 pellets formed in the co-ignimbrite plume fell into the density-stratified current and accreted
720 rims to become AP2 pellets that were then deposited in ignimbrite. After the current passed by, the remaining AP1
721 pellets fell from the co-ignimbrite plume to form a clast-supported overlying layer (Brown et al., 2010).

722
723 The atmosphere in the near-plume zone would have been rich in ash and electrically charged, with scope for
724 circulation towards and away from the hot plume axis and greater availability of water (originating for example
725 from entrainment of moist tropospheric air or phreatomagmatism) (Brown et al., 2012 and references therein). In
726 this proximal region ash aggregation can occur both within the vertical eruption plume and density-stratified
727 currents (e.g., Bonadonna et al., 2002), potentially leading to different types of accretionary pellets becoming
728 intermixed and deposited. The phase 2 proximal ash layer, which contains both AP1 and AP2 pellets of a similar
729 size, is interpreted to reflect fallout of aggregates derived from both the eruption plume and the co-ignimbrite cloud
730 of the first Poris PDC, at a time early in the eruption when PDC activity had ceased sufficiently for fragile
731 unstructured ash pellets to be deposited and preserved.

732 **7.4 The length of hiatus**

733 It is difficult to estimate how long proximal and distal hiatuses in PDC activity lasted during the Poris event, and
734 indeed how long the eruption itself lasted. Similar large-scale ignimbrites have been observed to derive from

735 sustained currents lasting for minutes to hours (e.g., Pinatubo, 1991; Scott et al., 1996). It is known that ash
736 aggregates can form quickly; AP1 aggregates were deposited within five minutes of the start of the 1990 eruption
737 of Sakurajima volcano in Japan (Gilbert & Lane, 1994). In 1997, during two Vulcanian explosions at Soufriere
738 Hills volcano, Montserrat produced an ashfall with a peak accumulation rate of $0.5\text{-}1.2 \times 10^{-3} \text{ kg m}^{-2} \text{ s}^{-1}$ (Bonadonna
739 et al., 2002). The ash fallout was accompanied by sedimentation of AP1 aggregates up to 4 mm in diameter, which
740 began 15 minutes after the onset of the eruptions and lasted for 10-30 minutes. It seems conceivable that the phase
741 2 ash layer, correlated across both proximal and distal regions, could represent a fundamental hiatus in PDC activity
742 of as little as tens of minutes, but possibly hours.

743

744 **8. Implications**

745 Evidence of unsteadiness and nonuniformity is common in both field studies and modelling of PDC activity (e.g.,
746 Doronzo et al., 2017; Andrews, 2019; G. Smith et al., 2020), with multiple factors at the vent, within the
747 surrounding environment and landscape, and spontaneously within the current itself (Rowley et al., 2023)
748 contributing to changes in behaviour at a range of spatial scales and timeframes. However, such changes in PDC
749 behaviour are rarely illustrated in stratigraphic architecture at regional scale, from vent to distal reaches, due to
750 lack of exposure.

751

752 This work reveals how correlation of distinct pyroclastic architecture deposited at different locations at the same
753 point in time can impact our interpretations of eruption history. The correlation illustrates that (1) hiatuses in PDC
754 activity recorded distally may not occur proximally, (2) hiatus in PDC activity can vary spatially (and potentially
755 rapidly) due to large-scale changes in PDC dynamics in time and space, and (3) entrachron correlation across an
756 ignimbrite sheet can reveal regional-scale PDC behaviours critical to our understanding of eruption history and
757 hazard. The study highlights the uncertainties inherent in interpretations made without the presence of proximal
758 stratigraphy, particularly when interpreting the number of pyroclastic density currents generated during a Plinian
759 event. It provides a direct potential link between stratigraphic relationships observed in the field, and spontaneous
760 behaviours observed in analogue experimental modelling that are difficult to observe during an eruption in real-
761 time. Future developments in analogue modelling of fluidised granular flows (for example, replicating waning
762 conditions) may provide insights that improve our understanding of the pulsatory PDC behaviours that generate
763 unique stratigraphy.

764

765 **Author contributions**

766 This study is based upon correlation carried out during NJD's PhD research, which draws on the PhD research of
767 RJB. NJD carried out proximal analysis, undertook correlative analysis, developed the concept and wrote the paper.
768 RJD carried out distal analysis, contributed to discussions and co-wrote the paper. PBK carried out distal sampling,
769 supervised both NJD and RJB and contributed to discussions.

770

771 **Acknowledgements**

772 NJD acknowledges Natural Environment Research Council studentship NE/G523855/1.

773

774 **Data availability**

775 All data presented in this work is available in full in the open access thesis of NJD located in a repository here:

776 <https://livrepository.liverpool.ac.uk/6253/>

777

778 **References**

- 779 Ancochea, E., Fuster, M., Ibarrola, E., Cendrero, A., Coello, J., Hernan, F., Cantagrel, J. M., & Jamond, C. (1990).
780 Volcanic evolution of the island of Tenerife (Canary Islands) in the light of new K-Ar data. In *Journal of*
781 *Volcanology and Geothermal Research*.
- 782 Ancochea, E., Huertas, M. J., Cantagrel, J. M., Coello, J., Fúster, J. M., Arnaud, N., & Ibarrola, E. (1999). Evolution
783 of the Cañadas edifice and its implications for the origin of the Cañadas Caldera (Tenerife, Canary Islands).
784 *Journal of Volcanology and Geothermal Research*, 88(3), 177–199.
785 [https://doi.org/https://doi.org/10.1016/S0377-0273\(98\)00106-1](https://doi.org/https://doi.org/10.1016/S0377-0273(98)00106-1)
- 786 Andrews, B. J. (2019). Recognizing unsteadiness in the transport systems of dilute pyroclastic density currents.
787 *Bulletin of Volcanology*, 81(2), 5. <https://doi.org/10.1007/s00445-018-1266-5>
- 788 Andrews, B. J., & Manga, M. (2011). Effects of topography on pyroclastic density current runout and formation of
789 coignimbrites. *Geology*, 39(12), 1099–1102. <https://doi.org/10.1130/G32226.1>
- 790 Aravena, A., & Roche, O. (2022). Influence of the topography of stratovolcanoes on the propagation and
791 channelization of dense pyroclastic density currents analyzed through numerical simulations. *Bulletin of*
792 *Volcanology*, 84(7), 67. <https://doi.org/10.1007/s00445-022-01576-2>

- 793 Báez, W., de Silva, S., Chiodi, A., Bustos, E., Giordano, G., Arnosio, M., Suzaño, N., Viramonte, J. G., Norini, G.,
794 & Groppelli, G. (2020). Pulsating flow dynamics of sustained, forced pyroclastic density currents: insights
795 from a facies analysis of the Campo de la Piedra Pómez ignimbrite, southern Puna, Argentina. *Bulletin of*
796 *Volcanology*, 82(7), 53. <https://doi.org/10.1007/s00445-020-01385-5>
- 797 Balmforth, N. J., & Mandre, S. (2004). Dynamics of roll waves. *Journal of Fluid Mechanics*, 514, 1–33.
798 <https://doi.org/DOI: 10.1017/S0022112004009930>
- 799 Bonadonna, C., Mayberry, G. C., Calder, E. S., Sparks, R. S. J., Choux, C., Jackson, P., Lejeune, A. M., Loughlin,
800 S. C., Norton, G. E., Rose, W. I., Ryan, G., & Young, S. R. (2002). Tephra fallout in the eruption of Soufrière
801 Hills Volcano, Montserrat. In *Geological Society, London, Memoirs* (Vol. 21, pp. 483–516).
802 <https://doi.org/10.1144/GSL.MEM.2002.021.01.22>
- 803 Branney, M. J., & Kokelaar, P. (1992). *A reappraisal of ignimbrite emplacement: progressive aggradation and*
804 *changes from particulate to non-particulate flow during emplacement of high-grade ignimbrite* (Vol. 54).
805 Springer-Verlag.
- 806 Branney, M. J., & Kokelaar, P. (1997). Giant bed from a sustained catastrophic density current flowing over
807 topography: Acatlán ignimbrite, Mexico. *Geology*, 25(2), 115–118. [https://doi.org/10.1130/0091-](https://doi.org/10.1130/0091-7613(1997)025<0115:GBFASC>2.3.CO;2)
808 [7613\(1997\)025<0115:GBFASC>2.3.CO;2](https://doi.org/10.1130/0091-7613(1997)025<0115:GBFASC>2.3.CO;2)
- 809 Branney, M. J., & Kokelaar, P. (2002). *Pyroclastic Density Currents and the Sedimentation of Ignimbrites*.
810 Geological Society of London. <https://doi.org/10.1144/GSL.MEM.2003.027>
- 811 Brown, R. J. (2001). *Eruption history and depositional processes of the poris ignimbrite of Tenerife and the*
812 *Glaramara Tuff of the English Lake District*.
813 [https://figshare.com/articles/Eruption_history_and_depositional_processes_of_the_poris_ignimbrite_of_Te-](https://figshare.com/articles/Eruption_history_and_depositional_processes_of_the_poris_ignimbrite_of_Tenerife_and_the_Glaramara_Tuff_of_the_English_Lake_District/10091993)
814 [nerife_and_the_Glaramara_Tuff_of_the_English_Lake_District/10091993](https://figshare.com/articles/Eruption_history_and_depositional_processes_of_the_poris_ignimbrite_of_Tenerife_and_the_Glaramara_Tuff_of_the_English_Lake_District/10091993)
- 815 Brown, R. J., Barry, T. L., Branney, M. J., Pringle, M. S., & Bryan, S. E. (2003). The Quaternary pyroclastic
816 succession of southeast Tenerife, Canary Islands: explosive eruptions, related caldera subsidence, and sector
817 collapse. *Geological Magazine*, 140(3), 265–288. <https://doi.org/DOI: 10.1017/S0016756802007252>
- 818 Brown, R. J., Bonadonna, C., & Durant, A. J. (2012). A review of volcanic ash aggregation. *Physics and Chemistry*
819 *of the Earth*, 45–46, 65–78. <https://doi.org/10.1016/j.pce.2011.11.001>
- 820 Brown, R. J., & Branney, M. J. (2004a). Bypassing and diachronous deposition from density currents: Evidence
821 from a giant regressive bed form in the Poris ignimbrite, Tenerife, Canary Islands. *Geology*, 32(5), 445–448.
822 <https://doi.org/10.1130/G20188.1>

- 823 Brown, R. J., & Branney, M. J. (2004b). Event-stratigraphy of a caldera-forming ignimbrite eruption on Tenerife:
824 The 273 ka Poris Formation. *Bulletin of Volcanology*, 66(5), 392–416. [https://doi.org/10.1007/s00445-003-](https://doi.org/10.1007/s00445-003-0321-y)
825 0321-y
- 826 Brown, R. J., & Branney, M. J. (2013). Internal flow variations and diachronous sedimentation within extensive,
827 sustained, density-stratified pyroclastic density currents flowing down gentle slopes, as revealed by the
828 internal architectures of ignimbrites on Tenerife. *Bulletin of Volcanology*, 75(7), 1–24.
829 <https://doi.org/10.1007/s00445-013-0727-0>
- 830 Brown, R. J., Branney, M. J., Maher, C., & Dávila-Harris, P. (2010). Origin of accretionary lapilli within ground-
831 hugging density currents: Evidence from pyroclastic couplets on Tenerife. *Bulletin of the Geological Society*
832 *of America*, 122(1–2), 305–320. <https://doi.org/10.1130/B26449.1>
- 833 Bryan, S. E., Cas, R. A. F., & Martí, J. (2000). The 0.57 Ma plinian eruption of the Granadilla Member, Tenerife
834 (Canary Islands): an example of complexity in eruption dynamics and evolution. In *Journal of Volcanology*
835 *and Geothermal Research* (Vol. 103). www.elsevier.nl/locate/jvolgeores
- 836 Bryan, S. E., Martí, J., & Cas, R. A. F. (1998). Stratigraphy of the Bandas del Sur Formation: an extracaldera record
837 of Quaternary phonolitic explosive eruptions from the Las Cañadas edifice, Tenerife (Canary Islands).
838 *Geological Magazine*, 135(5), 605–636. [https://doi.org/DOI: 10.1017/S0016756897001258](https://doi.org/DOI:10.1017/S0016756897001258)
- 839 Bursik, M. I., & Woods, A. W. (1996). The dynamics and thermodynamics of large ash flows. *Bulletin of*
840 *Volcanology*, 58, 175–193.
- 841 Cas, R. A. F., Porritt, L., Pittari, A., & Hayman, P. (2008). A new approach to kimberlite facies terminology using
842 a revised general approach to the nomenclature of all volcanic rocks and deposits: Descriptive to genetic.
843 *Journal of Volcanology and Geothermal Research*, 174(1), 226–240.
844 <https://doi.org/https://doi.org/10.1016/j.jvolgeores.2007.12.018>
- 845 Cas, R. A. F., Wolff, J. A., Martí, J., Olin, P. H., Edgar, C. J., Pittari, A., & Simmons, J. M. (2022). Tenerife, a
846 complex end member of basaltic oceanic island volcanoes, with explosive polygenetic phonolitic calderas,
847 and phonolitic-basaltic stratovolcanoes. *Earth-Science Reviews*, 230, 103990.
848 <https://doi.org/https://doi.org/10.1016/j.earscirev.2022.103990>
- 849 Cas, R. A. F., & Wright, J. V. (1987). Volcanic Successions Modern and Ancient. *Volcanic Successions Modern*
850 *and Ancient*. <https://doi.org/10.1007/978-94-009-3167-1>
- 851 Cavazos-Álvarez, J. A., & Carrasco-Núñez, G. (2020). Anatomy of the Xáltipan ignimbrite at Los Humeros
852 Volcanic Complex; the largest eruption of the Trans-Mexican Volcanic Belt. *Journal of Volcanology and*
853 *Geothermal Research*, 392, 106755. <https://doi.org/https://doi.org/10.1016/j.jvolgeores.2019.106755>

- 854 Charbonnier, S. J., Garin, F., Rodríguez, L. A., Ayala, K., Cancel, S., Escobar-Wolf, R., Chigna, G., Chun-Quinillo,
855 C., González, D., Chigna, W., Chun-Quinillo, K., Mérida, R., Juárez, F., & Calder, E. S. (2023). Unravelling
856 the dynamics and hazards of the June 3rd, 2018, pyroclastic density currents at Fuego volcano (Guatemala).
857 *Journal of Volcanology and Geothermal Research*, 436, 107791.
858 <https://doi.org/https://doi.org/10.1016/j.jvolgeores.2023.107791>
- 859 Dávila Harris, P., Branney, M. J., & Storey, M. (2011). Large eruption-triggered ocean-island landslide at Tenerife:
860 Onshore record and long-term effects on hazardous pyroclastic dispersal. *Geology*, 39(10), 951–954.
861 <https://doi.org/10.1130/G31994.1>
- 862 Dávila Harris, P., Branney, M. J., Storey, M., Taylor, R. N., & Sliwinski, J. T. (2023). The upper Pleistocene (1.8–
863 0.7 Ma) explosive eruptive history of Las Cañadas, ocean-island volcano, Tenerife. *Journal of Volcanology*
864 *and Geothermal Research*, 436, 107777. <https://doi.org/https://doi.org/10.1016/j.jvolgeores.2023.107777>
- 865 Dávila Harris, P., Ellis, B. S., Branney, M. J., & Carrasco-Núñez, G. (2013). Lithostratigraphic analysis and
866 geochemistry of a vitric spatter-bearing ignimbrite: the Quaternary Adeje Formation, Cañadas volcano,
867 Tenerife. *Bulletin of Volcanology*, 75(6), 722. <https://doi.org/10.1007/s00445-013-0722-5>
- 868 Doronzo, D. M., Dellino, P., Sulpizio, R., & Lucchi, F. (2017). Merging field mapping and numerical simulation
869 to interpret the lithofacies variations from unsteady pyroclastic density currents on uneven terrain: The case
870 of La Fossa di Vulcano (Aeolian Islands, Italy). *Journal of Volcanology and Geothermal Research*, 330, 36–
871 42. <https://doi.org/https://doi.org/10.1016/j.jvolgeores.2016.11.016>
- 872 Doronzo, D. M., Valentine, G. A., Dellino, P., & de Tullio, M. D. (2010). Numerical analysis of the effect of
873 topography on deposition from dilute pyroclastic density currents. *Earth and Planetary Science Letters*,
874 300(1), 164–173. <https://doi.org/https://doi.org/10.1016/j.epsl.2010.10.003>
- 875 Dowe, N., & Williams, R. (2022). Simultaneous fall and flow during pyroclastic eruptions: A novel proximal
876 hybrid facies. *Geology*, 50(10), 1187–1191. <https://doi.org/10.1130/G50169.1>
- 877 Druitt, T. H. (1998). Pyroclastic density currents. *Geological Society, London, Special Publications*, 145(1), 145–
878 182. <https://doi.org/10.1144/GSL.SP.1996.145.01.08>
- 879 Dufek, J., Esposti Ongaro, T., & Roche, O. (2015). Pyroclastic density currents: processes and models. Chapter 35.
880 *Part IV Explosive Volcanism, The Encyclopedia of Volcanoes*.
- 881 Edgar, C. J., Wolff, J. A., Nichols, H. J., Cas, R. A. F., & Martí, J. (2002). A complex Quaternary ignimbrite-
882 forming phonolitic eruption: the Poris Member of the Diego Hernández Formation (Tenerife, Canary Islands).
883 *Journal of Volcanology and Geothermal Research*, 118(1), 99–130.
884 [https://doi.org/https://doi.org/10.1016/S0377-0273\(02\)00252-4](https://doi.org/https://doi.org/10.1016/S0377-0273(02)00252-4)

- 885 Edgar, C. J., Wolff, J. A., Olin, P. H., Nichols, H. J., Pittari, A., Cas, R. A. F., Reiners, P. W., Spell, T. L., & Martí,
886 J. (2007). The late Quaternary Diego Hernandez Formation, Tenerife: Volcanology of a complex cycle of
887 voluminous explosive phonolitic eruptions. *Journal of Volcanology and Geothermal Research*, 160(1–2), 59–
888 85. <https://doi.org/10.1016/j.jvolgeores.2006.06.001>
- 889 Fierstein, J., Houghton, B. F., Wilson, C. J. N., & Hildreth, W. (1997). Complexities of plinian fall deposition at
890 vent: An example from the 1912 Novarupta eruption (Alaska). *Journal of Volcanology and Geothermal*
891 *Research*, 76(3–4), 215–227. [https://doi.org/10.1016/S0377-0273\(96\)00081-9](https://doi.org/10.1016/S0377-0273(96)00081-9)
- 892 Fierstein, J., & Wilson, C. J. N. (2005). Assembling an ignimbrite: Compositionally defined eruptive packages in
893 the 1912 Valley of Ten Thousand Smokes ignimbrite, Alaska. *GSA Bulletin*, 117(7–8), 1094–1107.
894 <https://doi.org/10.1130/B25621.1>
- 895 Fisher, R. V. (1966). Mechanism of deposition from pyroclastic flows. *American Journal of Science*, 264(5), 350–
896 363.
- 897 Fisher, R. V., Orsi, G., Ort, M., & Heiken, G. (1993). Mobility of a large-volume pyroclastic flow — emplacement
898 of the Campanian ignimbrite, Italy. *Journal of Volcanology and Geothermal Research*, 56(3), 205–220.
899 [https://doi.org/https://doi.org/10.1016/0377-0273\(93\)90017-L](https://doi.org/https://doi.org/10.1016/0377-0273(93)90017-L)
- 900 Fisher, R. V., & Schmincke, H.-U. (1984). Pyroclastic Flow Deposits. *Pyroclastic Rocks*, 186–230.
901 https://doi.org/10.1007/978-3-642-74864-6_8
- 902 Gase, A. C., Brand, B. D., & Bradford, J. H. (2017). Evidence of erosional self-channelization of pyroclastic density
903 currents revealed by ground-penetrating radar imaging at Mount St. Helens, Washington (USA). *Geophysical*
904 *Research Letters*, 44(5), 2220–2228. <https://doi.org/https://doi.org/10.1002/2016GL072178>
- 905 Gilbert, J. S., & Lane, S. J. (1994). The origin of accretionary lapilli. *Bulletin of Volcanology*, 56(5), 398–411.
906 <https://doi.org/10.1007/BF00326465>
- 907 Gooday, R. J., Brown, D. J., Goodenough, K. M., & Kerr, A. C. (2018). A proximal record of caldera-forming
908 eruptions: the stratigraphy, eruptive history and collapse of the Palaeogene Arran caldera, western Scotland.
909 *Bulletin of Volcanology*, 80(9), 70. <https://doi.org/10.1007/s00445-018-1243-z>
- 910 Houghton, B. F., Wilson, C. J. N., Fierstein, J., & Hildreth, W. (2004). Complex proximal deposition during the
911 Plinian eruptions of 1912 at Novarupta, Alaska. *Bulletin of Volcanology*, 66(2), 95–133.
912 <https://doi.org/10.1007/s00445-003-0297-7>
- 913 Johnson, C. G., Kokelaar, B. P., Iverson, R. M., Logan, M., LaHusen, R. G., & Gray, J. M. N. T. (2012). Grain-
914 size segregation and levee formation in geophysical mass flows. *Journal of Geophysical Research: Earth*
915 *Surface*, 117(F1). <https://doi.org/https://doi.org/10.1029/2011JF002185>

- 916 Kneller, B. C., & Branney, M. J. (1995). Sustained high-density turbidity currents and the deposition of thick
917 massive sands. *Sedimentology*, 42(4), 607–616. <https://doi.org/10.1111/J.1365-3091.1995.TB00395.X>
- 918 Kostaschuk, R., Nasr-Azadani, M. M., Meiburg, E., Wei, T., Chen, Z., Negretti, M. E., Best, J., Peakall, J., &
919 Parsons, D. R. (2018). On the Causes of Pulsing in Continuous Turbidity Currents. *Journal of Geophysical*
920 *Research: Earth Surface*, 123(11), 2827–2843. <https://doi.org/https://doi.org/10.1029/2018JF004719>
- 921 Lube, G., Breard, E. C. P., Esposti-Ongaro, T., Dufek, J., & Brand, B. (2020). Multiphase flow behaviour and
922 hazard prediction of pyroclastic density currents. *Nature Reviews Earth & Environment*, 1(7), 348–365.
923 <https://doi.org/10.1038/s43017-020-0064-8>
- 924 Lube, G., Cronin, S. J., Platz, T., Freundt, A., Procter, J. N., Henderson, C., & Sheridan, M. F. (2007). Flow and
925 deposition of pyroclastic granular flows: A type example from the 1975 Ngauruhoe eruption, New Zealand.
926 *Journal of Volcanology and Geothermal Research*, 161(3), 165–186.
927 <https://doi.org/https://doi.org/10.1016/j.jvolgeores.2006.12.003>
- 928 Martí, J. (2019). Las Cañadas caldera, Tenerife, Canary Islands: A review, or the end of a long volcanological
929 controversy. *Earth-Science Reviews*, 196, 102889.
930 <https://doi.org/https://doi.org/10.1016/j.earscirev.2019.102889>
- 931 Martí, J., Mitjavila, J., & Araña, V. (1994). Stratigraphy, structure and geochronology of the Las Cañadas caldera
932 (Tenerife, Canary Islands). *Geological Magazine*, 131(6), 715–727. [https://doi.org/DOI:](https://doi.org/DOI:10.1017/S0016756800012838)
933 10.1017/S0016756800012838
- 934 Martí, J., Mitjavila, J., & Villa, I. (1990). Stratigraphy and K-Ar ages of the Diego Hernandez wall and their
935 significance on the Las Cafiadas Caldera formation (Tenerife, Canary Islands). *Terra Nova*, 2(2), 148–153.
- 936 Mues-Schumacher, U., & Schumacher, R. (1996). Problems of Stratigraphic Correlation and New K-Ar Data for
937 Ignimbrites from Cappadocia, Central Turkey. *International Geology Review*, 38(8), 737–746.
938 <https://doi.org/10.1080/00206819709465357>
- 939 Myers, M. L., Wallace, P. J., Wilson, C. J. N., Morter, B. K., & Swallow, E. J. (2016). Prolonged ascent and
940 episodic venting of discrete magma batches at the onset of the Huckleberry Ridge supereruption, Yellowstone.
941 *Earth and Planetary Science Letters*, 451, 285–297. <https://doi.org/10.1016/J.EPSL.2016.07.023>
- 942 Pittari, A., Cas, R. A. F., Edgar, C. J., Nichols, H. J., Wolff, J. A., & Martí, J. (2006). The influence of
943 palaeotopography on facies architecture and pyroclastic flow processes of a lithic-rich ignimbrite in a high
944 gradient setting: The Abrigo Ignimbrite, Tenerife, Canary Islands. *Journal of Volcanology and Geothermal*
945 *Research*, 152(3–4), 273–315. <https://doi.org/10.1016/j.jvolgeores.2005.10.007>

- 946 Pollock, N. M., Brand, B. D., Rowley, P. J., Sarocchi, D., & Sulpizio, R. (2019). Inferring pyroclastic density
947 current flow conditions using syn-depositional sedimentary structures. *Bulletin of Volcanology*, *81*(8), 1–16.
948 <https://doi.org/10.1007/S00445-019-1303-Z/FIGURES/7>
- 949 Ross, C. S., & Smith, R. L. (1961). Ash-flow tuffs: Their origin, geologic relations, and identification. In
950 *Professional Paper*. <https://doi.org/10.3133/pp366>
- 951 Rowley, P., Williams, R., Johnson, M., Johnston, T., Dowey, N., Parson, D. P., Provost, A., Roche, O., Smith, G.
952 M., & Walding, N. (2023). Spontaneous Unsteadiness and Sorting in Pyroclastic Density Currents and their
953 Deposits. *EarthArxiv Preprint*.
- 954 Scott, W. E., Hoblitt, R. P., Torres, R. C., Self, S., Martinez, M. L., & Nillos, T. J. (1996). Pyroclastic flows of the
955 June 15 1991, climactic eruption of Mount Pinatubo. In C. G. Newhall & S. Punongbayan (Eds.), *Fire and*
956 *mud: eruptions of Pinatubo, Philippines* (pp. 545–570). University of Washington Press.
- 957 Sigurdsson, H., & Carey, S. (1989). Plinian and co-ignimbrite tephra fall from the 1815 Tambora eruption. *Bulletin*
958 *of Volcanology*, *51*(4), 243–270. <https://doi.org/10.1007/BF01073515>
- 959 Silva Parejas, C., Druitt, T. H., Robin, C., Moreno, H., & Naranjo, J.-A. (2010). The Holocene Pucón eruption of
960 Volcán Villarrica, Chile: deposit architecture and eruption chronology. *Bulletin of Volcanology*, *72*(6), 677–
961 692. <https://doi.org/10.1007/s00445-010-0348-9>
- 962 Smith, G., Rowley, P., Williams, R., Giordano, G., Trolese, M., Silleni, A., Parsons, D. R., & Capon, S. (2020). A
963 bedform phase diagram for dense granular currents. *Nature Communications*, *11*(1), 1–11.
964 <https://doi.org/10.1038/s41467-020-16657-z>
- 965 Smith, N. (2012). *Near-vent processes of the 273 ka Poris eruption (Tenerife)* [Unpublished Thesis, University of
966 Liverpool]. <https://livrepository.liverpool.ac.uk/6253/>
- 967 Smith, N., & Kokelaar, B. P. (2013). Proximal record of the 273 ka Poris caldera-forming eruption, Las Cañadas,
968 Tenerife. *Bulletin of Volcanology*, *75*(11), 768–789. <https://doi.org/10.1007/s00445-013-0768-4>
- 969 Soriano, C., Galindo, I., Martí, J., & Wolff, J. (2006). Conduit-vent structures and related proximal deposits in the
970 Las Cañadas caldera, Tenerife, Canary Islands. *Bulletin of Volcanology*, *69*(2), 217–231.
971 <https://doi.org/10.1007/s00445-006-0069-2>
- 972 Sparks, R. S. J. (1976). Grain size variations in ignimbrites and implications for the transport of pyroclastic flows.
973 *Sedimentology*, *23*(2), 147–188. <https://doi.org/https://doi.org/10.1111/j.1365-3091.1976.tb00045.x>
- 974 Sparks, R. S. J., Self, S., & Walker, G. P. L. (1973). Products of Ignimbrite Eruptions. *Geology*, *1*(3), 115–118.
975 [https://doi.org/10.1130/0091-7613\(1973\)1<115:POIE>2.0.CO;2](https://doi.org/10.1130/0091-7613(1973)1<115:POIE>2.0.CO;2)

- 976 Sparks, R. S. J., & Walker, G. P. L. (1977). The significance of vitric-enriched air-fall ashes associated with crystal-
977 enriched ignimbrites. *Journal of Volcanology and Geothermal Research*, 2(4), 329–341.
978 [https://doi.org/https://doi.org/10.1016/0377-0273\(77\)90019-1](https://doi.org/https://doi.org/10.1016/0377-0273(77)90019-1)
- 979 Sulpizio, R., Dellino, P., Doronzo, D. M., & Sarocchi, D. (2014). Pyroclastic density currents: state of the art and
980 perspectives. *Journal of Volcanology and Geothermal Research*, 283, 36–65.
981 <https://doi.org/10.1016/J.JVOLGEORES.2014.06.014>
- 982 Watkins, S. D., Giordano, G., Cas, R. A. F., & De Rita, D. (2002). Emplacement processes of the mafic Villa Senni
983 Eruption Unit (VSEU) ignimbrite succession, Colli Albani volcano, Italy. *Journal of Volcanology and
984 Geothermal Research*, 118(1), 173–203. [https://doi.org/https://doi.org/10.1016/S0377-0273\(02\)00256-1](https://doi.org/https://doi.org/10.1016/S0377-0273(02)00256-1)
- 985 Williams, R., Branney, M. J., & Barry, T. L. (2014). Temporal and spatial evolution of a waxing then waning
986 catastrophic density current revealed by chemical mapping. *Geology*, 42(2), 107–110.
987 <https://doi.org/10.1130/G34830.1>
- 988 Wilson, C. J. N. (1985). The Taupo eruption, New Zealand. II. The Taupo Ignimbrite. *Philosophical Transactions
989 of the Royal Society of London. Series A, Mathematical and Physical Sciences*, 314(1529), 229–310.
990 <https://doi.org/10.1098/RSTA.1985.0020>
- 991 Wilson, C. J. N., & Hildreth, W. (1997). The Bishop Tuff: New Insights from Eruptive Stratigraphy. *The Journal
992 of Geology*, 105(4), 407–440. <https://doi.org/10.1086/515937>
- 993 Wilson, C. J. N., & Hildreth, W. (1998). Hybrid fall deposits in the Bishop Tuff, California: A novel pyroclastic
994 depositional mechanism. *Geology*, 26(1), 7–10.
995